Bull. Chem. Soc. Jpn., 70, 3137—3152 (1997)

Syntheses and Crystal Structures of ET and BETS Salts Containing Bis(dithiosquarato)metalate Anions

Hisashi Tanaka, Akiko Kobayashi,* and Hayao Kobayashi†

Department of Chemistry, School of Science, The University of Tokyo, Hongo, Bunkyo-ku, Tokyo 113

†Institute for Molecular Science, Myodaiji-cho, Okazaki 444

(Received May 6, 1997)

A series of cation radical salts of bis(ethylenedithio)tetrathiafulvalene (ET) and bis(ethylenedithio)-tetraselenafulvalene (BETS) as donors and bis(dithiosquarato)metalate ($[M(dts)_2]^{n-}$) as anions were synthesized. The electrical resistivities of most of these salts ($(BETS)_2[Pd(dts)_2]$ (**1**), $(BETS)_2[Pd(dts)_2]\cdot 2(1,1,2,2\text{-TCE})$ (**2**) (1,1,2,2-TCE=1,1,2,2−tetrachloroethane), $(BETS)[Au(dts)_2]$ (**4**), $(ET)_2[Pd(dts)_2]$ (**5**), $(ET)_2[Pt(dts)_2]$ (**6**), and $(ET)[Au(dts)_2]$ (**7**)) were semiconductive. However, one of the BETS salts with $[Pd(dts)_2]$, whose donor : anion ratio was 5 : 1. $(BETS)_x[Pd(dts)_2]$ ($x\approx 5.0$) (**3**), showed a metallic behavior down to 4 K. Although the crystal structure of these semiconducting salts was a kind of mixed stacks, many short contacts within the sum of the van der Waals radii were seen between chalcogens of the donors, and between chalcogens of the donor and anion. In addition, four terminal oxygen atoms of bis(dithiosquarato)metalate anion had C–H···O hydrogen bonds with terminal ethylene groups of ET and BETS, which was one of the factors determining the conformation of the terminal ethylene groups in these crystals.

Bis(ethylenedithio)tetrathiafulvalene abbreviated as BEDT−TTF or ET (Fig. 1), and bis(ethylenedithio)-tetraselenafulvalene, abbreviated as BETS (Fig. 1), are known as good donors, because they cause many molecular superconductors and stable metallic salts down to very low temperature.[1—4] In particular, some organic conductors containing 3d magnetic transition-metal complex anions show interesting electric and magnetic properties. In the case of organic conductors with closed-shell anions, such as ClO_4^-, PF_6^-, etc., the electrical properties of the system are determined only by the π-donor molecules, despite the fact that the anions play essential roles in constructing the crystal structures.

On the other hand, in charge-transfer salts with metal complex anions, both the π-donor molecules and transition-metal complex anions take part in determining the electrical properties. Furthermore, in these systems, not only electrically, but also magnetically, active natures can be expected. λ-$(BETS)_2FeCl_4$ is a good example of organic conductors containing a magnetic transition metal anion.[5] Unlike λ-type BETS superconductors with non-magnetic tetrahalide gallium ions ($T_c \leq 10$ K),[6] λ-$(BETS)_2FeCl_4$ exhibits a coupled metal-insulator and antiferromagnetic transition, which takes place at 8.5 K. Since the distances between iron atoms are larger than 6.2 Å, a direct dipole–dipole interaction is too small to give a magnetic interaction with a Weiss temperature of 15 K. Thus, the antiferromagnetic interaction responsible for magnetic ordering is suggested to be mediated via BETS molecules. Although the precise mechanism of a π-electron mediated spin–spin interaction is not clear at present, the π-d interaction can be controlled to some extent if we use magnetic transition metals having planar π ligands.

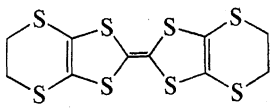

BEDT-TTF (ET)

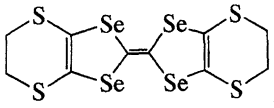

BEDT-TSF (BETS)

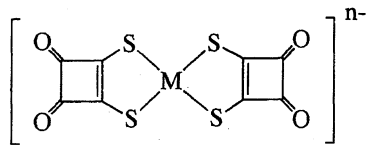

Bis(dithiosquarato) metalate ($[M(dts)_2]^{n-}$)
M = Ni, Pd, Pt, Mn, Fe, Co, Cu (n = 2),
Au (n = 1)

Fig. 1. Structures of (a) ET, (b) BETS, and (c) bis(dithiosquarate)metalate.

Compared with the traditional molecular conductors, in which conduction pathways are formed only from planar π-donor molecules and closed-shell counter ions, the charge-transfer salts with metal complex anions, such as (TTF)-$[Ni(dmit)_2]_2$,[7,8] α-(EDT-TTF)$[Ni(dmit)_2]$,[7,9,10] and (ET)[Ni-

$(dmit)_2]$,[11] have unique crystal structures and physical properties. In these systems, both the π-donor and π-acceptor molecules can principally take part in the formation of conduction bands.

However, the variety of these systems investigated so far has been rather limited. In an exploration of new types of molecular conducting systems with planar multi-chalcogen π-donor and π-acceptor molecules, we examined a series of cation radical salts of BEDT–TTF and BETS containing bis(dithiosquarato)metalate anions, $[M(dts)_2]^{n-}$ (M=Ni, Pd, Pt, Mn, Fe, Co, Cu, $n=2$; M=Au, $n=1$) (Fig. 1).

The syntheses of bis(dithiosquarato)metalates was reported by D. Coucouvanis et al. in 1974.[12,13] Bis(dithiosquarato)metalates of Ni^{II}, Pd^{II}, Pt^{II}, and Au^{III} are planar complexes, and bis(dithiosquarato)metalates of metals of Mn^{II}, Fe^{II}, Co^{II}, and Cu^{II} are complexes including magnetic transition-metals. Seven trials for the synthesis of conductors based on squarate-derivative metalate have been examined. The polymeric tetrathiosquarato complexes of nickel-group metals were prepared by Götzfried et al., which possess resistivities of 10^4—10^7 Ω cm at room temperature.[14] The molecular conductor consists of a planar complex; potassium bis(dithiosquarato)palladate was reported in 1987.[15] The $[Pd(dts)_2]$ molecules made stacked columns separated by potassium cations and water molecules, but showed a semi-conductive behavior and high resistivity at room temperature ($\rho_{rt}=5\times10^6$ Ω cm). We thus used ET and BETS as donors and the bis(dithiosquarato)metalates as anions.

Furthermore, the molecular sizes of bis(dithiosquarato)-metalates are almost the same as those of the donor molecules, ET and BETS, and it may be possible to produce various molecular stacking patterns different from most of the cation radical salts with simple anions, such as Cl^-, I_3^-, BF_4^-, PF_6^-, etc. The crystal structure of these cation radical salts with simple anions generally comprises two independent layers: one is the donor molecule layer (conducting part); the other is the anion layer (anions packed in open spaces). However, the bis(dithiosquarato)metalate anion is too large to be packed only in the open space of the donor stackings, and requires new stacking patterns of the donor and anion molecules. In addition, the bis(dithiosquarato)-metalate anion has four sulfur atoms and four oxygen atoms in its periphery, and many intermolecular contacts between chalcogens of bis(dithiosquarato)metalate anions and the donors are expected. Further, the four terminal oxygen atoms can interact with the terminal ethylene groups of ET and BETS, and a C–H···O weak hydrogen bond can construct multidimensional networks between columns in addition to the chalcogen–chalcogen contacts in these crystals.

Experimental

Synthesis. All of the procedures were performed under an inert atmosphere, and all of the solvents were or reagent grade and freshly distilled. ET and squaric acid were used as purchased from Tokyo Chemical Industry Co., Ltd. BETS was prepared according to literature methods,[16] and recrystallized from carbon disulfide. Potassium 1,2-cyclobutanedione-3,4-dithiolate (potassium dithiosquarate; K_2 dts) was prepared from squaric acid, and metal complexes of dithiosquarato ligands were prepared as potassium bis(dithiosquarato)metalates according to literature methods.[13,17,18] Tetraalkylammonium bis(dithiosquarato)metalates were prepared by mixing $K_n[M(dts)_2]$ (M=Au, $n=1$; M=Ni, Pd, Pt, Mn, Fe, Co, Cu, $n=2$) dissolved in ethanol and tetraalkylammonium bromide dissolved in acetone. The synthesis of tetra(*n*-butyl)ammonium bis(dithiosquarato)palladate was shown to be a typical procedure for synthesizing these compounds.

Tetra(*n*-buthyl)ammonium bis(dithiosquarato)palladate: A solution of 2.22 g potassium dithiosquarate in 2 ml of water was added to a suspension of 0.89 g paladium dichloride in 3 ml of water with vigorous stirring. A solution turned dark violet and a green microcrystalline was precipitated immediately. The product was filtered off, and washed with a small amount of ethanol under an inert atmosphere. After a 20 ml acetone solution of 0.85 g green microcrystalline was added into a 10 ml ethanol solution of 1.16 g tetra(*n*-buthyl)ammonium bromide,a complex was obtained as pale-green platelike crystals. Yield 0.90 g.

$(n\text{-}Bu_4N)_2[Pd(dts)_2]$: IR 1832, 1734, 1696, 1420, 1166, 918, 878, 540, 520 cm^{-1}. UV (acetonitrile) $\lambda_{max}=279$ nm, $\varepsilon_{max}=4.2\times10^4$. Anal. Calcd for $C_{40}H_{72}N_2O_4S_4Pd$: C, 54.61; H, 8.25; N, 3.18; S, 14.58%. Found: C, 54.46; H, 8.34; N, 3.20; S, 14.70%. The IR, UV-vis and elemental analysis data of $(Et_4N)_2[Pt(dts)_2]$ and $(Et_4N)[Au(dts)_2]$ were given as follows:

$(Et_4N)_2[Pt(dts)_2]$ IR 1834, 1726, 1686, 1408, 1170, 918, 880, 540, 528 cm^{-1}. UV (acetonitrile) $\lambda_{max}=228$ nm, $\varepsilon_{max}=3.8\times10^4$. Anal. Calcd for $C_{24}H_{40}N_2O_4S_4Pt$: C, 38.75; H, 5.42; N, 3.77; S, 17.24%. Found: C, 38.59; H, 5.54; N, 3.78; S, 17.08%.

$(Et_4N)[Au(dts)_2]$ IR 1816, 1760, 1734, 1408, 1382, 1144, 904, 742, 516 cm^{-1}. UV (acetonitrile) $\lambda_{max}=301$ nm, $\varepsilon_{max}=4.3\times10^4$. Anal. Calcd for $C_{16}H_{20}NO_4S_4Au$: C, 31.22; H, 3.27; N, 2.28; S, 20.84%. Found: C, 31.08; H, 3.13; N, 2.40; S, 20.90%.

Each cation radical salt was obtained by electrocrystallizations of the ET or BETS donor (5—8 mg) in solvents (20 ml) containing tetraalkylammonium bis(dithiosquarato)metalates or potassium bis-(dithiosquarato)metalates as electrolytes (40—50 mg). The detailed conditions of electrocrystallizations are summerized in Table 1. The ratios of the donor : anion of salts **1**, **2**, **4**, **5**, **6**, **7** were determined from the result of X-ray crystal structure determinations. Crystals of the cation radical salts ET and BETS with $[M(dts)_2]^{2-}$ (M=Ni, Mn, Fe Co, Cu) and BETS with $[Pt(dts)_2]^{2-}$ were not obtained.

The composition of salt **3** was analyzed by electron-probe microanalysis (JOEL-T-220, SED 8600). The calculated value is $(BETS)_5[Pd(dts)_2]$, S : Se : Pd = 53.3 : 44.4 : 2.2 (%), and the observed value, S : Se : Pd = 53.6 : 44.3 : 2.1 (%).

Crystal Structure Determination. All of the X-ray crystal data were collected by four-circle diffractometers (Rigaku AFC-5R or AFC-6S) at room temperature. Monochromated Mo $K\alpha$ radiation ($\lambda=0.7107$ Å) was used in all of the X-ray experiments. All of their crystal data and experimental details are listed in Table 2. Only the structure of salt **3** was not determined. The molecular structures and atomic coordinates of the other salts are shown in Fig. 2 and Table 3. All of the calculations were performed by direct methods and completed by Fourier techniques.[19] The non-hydrogen atoms were refined anisotropically, and hydrogen atoms were included, but not refined. The complete F_o-F_c data are deposited as Document No. 70047 at the Office of the Editor of Bull. Chem. Soc. Jpn.

Electrical Resistivity. The electrical resistivities were measured by a conventional four-probe method from room temperature to 77 or 4 K. Gold wires (ϕ 0.015 mm) were bonded to the crys-

Table 1. Detailed Conditions of Electrocrystallizations

	Donor	Electrolyte	Crystal appearance (donor : anion)[a]	Solvent, Condition, etc.
1	BETS	$(Bu_4N)_2[Pd(dts)_2]$	Black plates (2 : 1)	90% PhCl–10% MeCN, 0.2 μA, 17 days
2	BETS	$(Bu_4N)_2[Pd(dts)_2]$	Black plates (2 : 1)	90% 1,1,2,2-TCE–10% MeCN, 1.0—1.4 μA, 17 days, Containning 1,1,2,2-TCE as solvent for crystallization.
3	BETS	$(Bu_4N)_2[Pd(dts)_2]$	Black plates (5 : 1)	90% PhCl–10% MeCN, 0.14 μA, 7 days
4	BETS	$(Et_4N)[Au(dts)_2]$	Dark-red needles (1 : 1)	90% PhCl–10% EtOH, 0.04—0.2 μA, 9 days
5	ET	$(Et_4N)_2[Pd(dts)_2]$	Black needles (2 : 1)	90% 1,1,2-TCE–10% MeCN, 1.0—1.4 μA, 60 days
6	ET	$K_2[Pt(dts)_2]$	Black needles (2 : 1)	1,1,2-TCE, 18-Crown-6, 1.2 μA, 40 days
7	ET	$(Et_4N)[Au(dts)_2]$	Dark-red-needles (1 : 1)	90% 1,1,2-TCE–10% MeCN, 1.0—1.4 μA, 60 days

PhCl = Chlorobenzene, EtOH = Ethanol, MeCN = Acetonitrile, 1,1,2,2-TCE = 1,1,2,2-Tetrachloroethane, 1,1,2-TCE = 1,1,2-Trichloroethane. a) The ratios of donor : anion of the salts **1**, **2**, **4**, **5**, **6**, **7** were determined from the result of X-ray crystal structure determination. Only the ratio of the salt **3** was determined by electron probe microanalysis.

tals with conducting gold paste. Some samples were measured by pellets, because they were microcrystals and very fragile.

X-Ray Photoelectron Spectroscopy (XPS). The XPS spectrum was measured at room temperature with a Rigaku XPS-7000. Mg $K\alpha$ (1253.6 eV) radiation was used as the X-ray source. The pass energy was 15 eV for spectrum scanning. The binding energy was calibrated by assuming the measured binding energy of the Au $4f_{7/2}$ core level of gold plate to be 83.8 eV.[20] Sample compounds were reduced to powder and fixed on a sample holder with conductive tape. The scanning range was 99—75 eV for Au complexes, 352—327 eV for Pd complexes, 86—63 eV for Pt complexes.

Cyclic Voltammetry and Chronocoulometry. The electrochemical properties of $(Bu_4N)_2[Pd(dts)_2]$, $(Bu_4N)_2[Pt(dts)_2]$, and $(Bu_4N)[Au(dts)_2]$ were investigated by cyclic voltammetry and chronocoulometry (bulk electrolysis) with a BAS CV-50 W. The working electrode and the counter electrode were platinum, and the reference electrode was Ag/Ag^+ prepared by 0.1 mol dm^{-3} $AgNO_3$ and 0.1 mol dm^{-3} TBAP (= tetrabutylammonium perchlorate) dissolved in acetonitrile. As for the cyclic voltammetry measurement, each sample concentration was 0.01 mol dm^{-3} dissolved in 0.1 mol dm^{-3} TBAP/acetonitrile. The scan rates were at 0.1 V s^{-1}, and all measurements were carried out over the potential range −2.0 to +2.0 V. The reversible redox wave of ferrocene/ferrocenium ion was observed at 0.22 V v.s. Ag/Ag^+ electrode. The redox potential v.s. Ag/Ag^+ was transformed into the potential v.s. SCE by adding the potential difference between the Ag/Ag^+ electrode and the SCE, which was directly measured: $E_{SCE} = E_{Ag/Ag^+} - (0.22 \pm 0.03)$ V. As for chronocoulometry, each sample concentration was 0.001 mol dm^{-3} dissolved in 0.1 mol dm^{-3} TBAP/acetonitrile, and the potentiometer was set at a 0.20 V higher (or lower) potential than their observed oxidation (reduction) potential.

Optical Absorption. The optical absorptions of finely ground KBr pellet samples with a weight concentration of ca. 1% were measured with a Hitachi U-3500 spectrophotometer (3200—50000 cm^{-1}).

Results and Discussions

Molecular Structures. Selected bond lengths and bond angles of salts **1**, **2**, **4**, **5**, **6**, and **7** are given in Table 4. As compared with neutral ET and BETS, the C–Se bond lengths (1.90 Å, average) of BETS are about 0.14 Å longer than the C–S bond lengths (1.76 Å, average) of ET.[21,22] Since the selenium atoms of BETS protrude toward the short molecular axis, the side-by-side interactions between the BETS molecules are stronger than those of the ET molecules.[22] Although both ET and BETS are almost planar molecules, their terminal ethylene groups are flexible and take two types of conformations, "staggered" and "eclipsed". Figure 3 shows schematic drawings of six-membered-ring of ET and BETS. In the staggered conformation, each carbon of the terminal ethylene is located on a different side of the donor molecular plane. In the eclipsed conformation, both carbons are located on the same side. Every ET and BETS has two ethylene groups on both terminals. Both ethylene groups of salts **1**, **5**, and **6** take the eclipsed conformation, and both ethylene groups of salts **4** and **7** take the staggered conformation, while each ethylene group of salt **2** takes the eclipsed and staggered conformations. The ethylene groups in the eclipsed conformation bend remarkably, and the carbon atoms of the ethylene group are deviated from its donor molecular plane by more than 1.0 Å.

The structure of the dithiosquarate ligand is thought to be almost planar, because some squarate-derivative ligands, such as tetrathiasquarate, are planar molecule.[23] Thus the bis(dithiosquarato)metalates (M = Pd, Pt, Au) become a planar molecule.[12,13,15] The metal atom is coordinated in a planar fashion by the sulfur atoms of two dithiosquarate ligands. The metal–sulfur bond lengths (metal = Pd, Pt, Au) are almost similar (2.32—2.34 Å), and all of the bis(dithiosquarato)-metalates anions have similar molecular sizes. Moreover, the molecular size of $[M(dts)_2]$ (13.3×7.0×3.7 Å), estimated from the result of an X-ray crystal structure determination and van der Waals radii, is almost similar to those of ET (14.5×7.2×3.7 Å) and BETS (15.2×7.2×4.0 Å). In Fig. 4, the possible resonance forms of the dithiosquarate ligand are shown. From the results of a single-crystal X-ray struc-

Table 2. Crystal Data and Experimental Details

	(1) (BETS)$_2$[Pd(dts)$_2$]	(2) (BETS)$_2$[Pd(dts)$_2$] ·2(1,1,2,2-TCE)	(3) (BETS)$_x$[Pd(dts)$_2$] ($x \approx 5$)	(4) (BETS)[Au(dts)$_2$]	(5) (ET)$_2$[Pd(dts)$_2$]	(6) (ET)$_2$[Pt(dts)$_2$]	(7) (ET)[Au(dts)$_2$]
Formula	$C_{28}H_{16}O_4S_{12}Se_8Pd$	$C_{32}H_{20}O_4S_{12}Se_8PdCl_8$		$C_{18}H_8O_4S_8Se_4Au$	$C_{28}H_{16}O_4S_{20}Pd$	$C_{28}H_{16}O_4S_{20}Pt$	$C_{18}H_8O_4S_{12}Au$
Temperature/K	293	296	296	296	293	296	296
Formula mass	1539.23	1874.93		1057.59	1164.03	1252.72	869.95
Crystal system	Monoclinic	Monoclinic	Monoclinic	Triclinic	Monoclinic	Monoclinic	Triclinic
a/Å	8.512(4)	17.954(6)	11.952(2)	8.036(2)	13.33(2)	13.285(5)	12.132(3)
b/Å	27.849(6)	13.468(5)	4.159(2)	14.112(4)	11.181(9)	11.171(6)	14.438(6)
c/Å	8.938(5)	10.896(3)	18.708(3)	5.886(2)	14.371(8)	14.371(5)	8.116(5)
α/°				91.99(3)			100.79(2)
β/°	108.69(3)	90.11(3)	106.24(1)	97.00(2)	113.72(5)	113.58(2)	108.92(2)
γ/°				104.79(3)			68.71(2)
V/Å^3	2007(1)	2634(1)	892.8(6)	639.1(3)	1960(2)	1954(1)	1249.2(6)
Space group	$P2_1/c$ (#14)	$P2_1/c$(#14)		$P\bar{1}$ (#2)	$P2_1/a$ (#14)	$P2_1/a$ (#14)	$P\bar{1}$(#2)
Z	2	2		1	2	2	2
D_{calcd}	2.547	2.363		2.748	1.971	2.128	2.313
Crystal dimensions/mm	0.20 × 0.40 × 0.10	0.20 × 0.10 × 0.60	0.30 × 0.01 × 0.40	0.20 × 0.10 × 0.40	0.40 × 0.10 × 0.40	1.00 × 0.30 × 0.10	0.20 × 0.10 × 0.20
Radiation	Mo $K\alpha$ (λ = 0.71069 Å)	Mo $K\alpha$ (λ = 0.71069 Å)	Mo $K\alpha$ (λ = 0.71069 Å)	Mo $K\alpha$ (λ = 0.71069 Å)	Mo $K\alpha$ (λ = 0.71069 Å)	Mo $K\alpha$ (λ = 0.71069 Å)	Mo $K\alpha$ (λ = 0.71069 Å)
F_{000}	1452.00	1780.00		491.00	1164.00	1228.00	838.00
μ(Mo $K\alpha$)/cm^{-1}	83.81	67.99		121.54	15.77	46.82	69.41
Diffractometer	Rigaku AFC-5R	Rigaku AFC-5R		Rigaku AFC-5R	Rigaku AFC-6S	Rigaku AFC-6S	Rigaku AFC-5R
Scan type	ω	ω–2θ		ω–2θ	ω–2θ	ω–2θ	ω–2θ
Scan rate/deg min^{-1}	8.0	8.0		8.0	8.0	4.0	8.0
Scan width/°	1.00+0.30 tan θ	1.21+0.30 tan θ		1.31+0.30 tan θ	0.94+0.30 tan θ	1.10+0.30 tan θ	1.10+0.30 tan θ
Reflection obsd	5015	6529		3975	4927	4929	6013
Unique reflection	4719	6337		3725	4735	4733	5743
2θ range	6.0—55.0	6.0—55.0		6.0—60.0	6.0—55.0	6.0—55.0	6.0—55.0
Corrections	Lorentz-polarization Absorption	Lorentz-polarization Absorption		Lorentz-polarization Absorption	Lorentz-polarization Absorption	Lorentz-polarization Absorption	Lorentz-polarization Absorption
(trans. factors)	(0.4682—1.0000)	(0.4852—1.0000)		(0.4825—1.0000)	(0.6852—1.0000)	(0.4022—1.0000)	(0.4475—1.0000)
Solution	Direct method (SHELXS86)	Direct method (SAPI91)		Direct method (SHELXS86)	Direct method (SHELXS86)	Direct method (SAPI91)	Direct method (SHELXS86)
Refinement	Full-matrix least-squares	Full-matrix least-squares		Full-matrix least-squares	Full-matrix least-squares	Full-matrix least-squares	Full-matrix least-squares
N_r ($I > 3.00\sigma(I)$)	2090	2214		2123	2421	2655	3621
N_p	241	295		160	241	252	319
R; R_w	0.074; 0.068	0.054; 0.040		0.063; 0.047	0.044; 0.035	0.098; 0.111	0.034; 0.025
Goodness of fit	2.69	1.62		2.19	1.52	5.03	1.55
Max shift	0.16	0.06		0.20	0.20	0.03	0.22
Maximum peak in final diff. map (e$^-$ Å^{-3})	1.70	1.20		3.17	0.60	7.59	1.36

N_r = number of reflections, N_p = number of refined parameters, $R = \Sigma||F_o| - |F_c||/\Sigma|F_o|$, $R_w = [\Sigma w(|F_o| - |F_c|)^2/\Sigma|F_o|^2]^{1/2}$, goodness of fit = $[\Sigma w(|F_o| - |F_c|)^2/(N_r - N_p)]^{1/2}$, $w^{-1} = (\sigma^2(F_o) + g(F_o)^2)$.

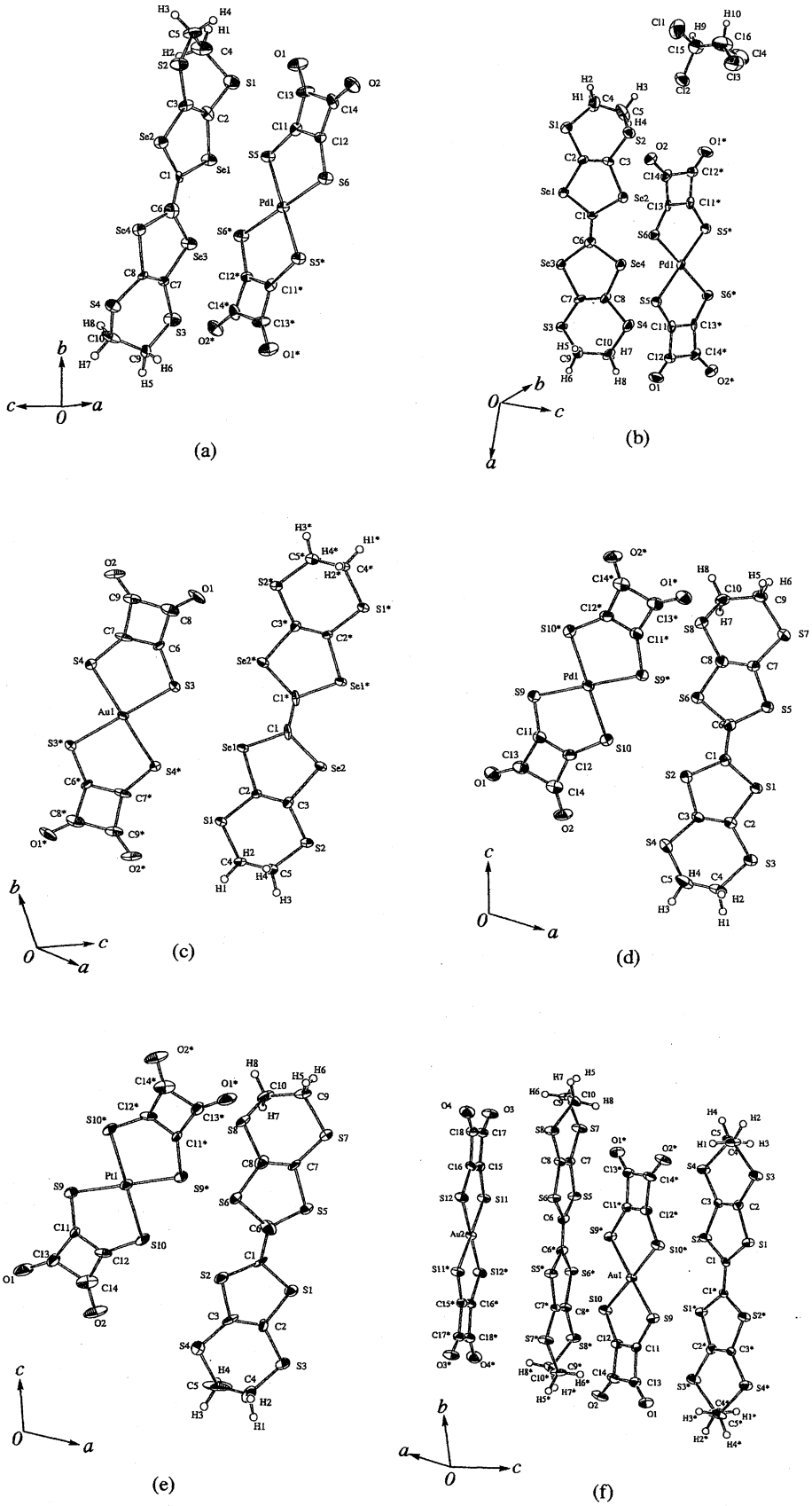

Fig. 2. ORTEP drawing and atomic labeling of the cation radical salts **1**, **2**, **4**, **5**, **6**, and **7**. Thermal elipsoids are drawn at the 35% probability level. The atom labeling with asterisk indicates crystallographic equivalent atoms, which are plotted by symmetry operation $(-x, -y, -z)$. (a) $(BETS)_2[Pd(dts)_2]$ (**1**), (b) $(BETS)_2[Pd(dts)_2]\cdot 2(1,1,2,2\text{-TCE})$ (**2**), (c) $(BETS)[Au(dts)_2]$ (**4**), (d) $(ET)_2[Pd(dts)_2]$ (**5**), (e) $(ET)_2[Pt(dts)_2]$ (**6**), (f) $(ET)[Au(dts)_2]$ (**7**).

Table 3. Atomic Coordinations and B_{eq} of Cation Radical Salts **1**, **2**, **4**, **5**, **6**, and **7**

(BETS)$_2$[Pd(dts)$_2$] (**1**)

Atom	x/a	y/b	z/c	B_{eq}/Å^2
Pd(1)	0.5000	0.5000	0.0000	2.01(4)
Se(1)	0.6807(2)	0.56968(8)	0.3775(3)	2.91(5)
Se(2)	0.9747(3)	0.60036(8)	0.6800(3)	2.85(5)
Se(3)	0.7258(2)	0.45618(8)	0.4835(3)	3.02(5)
Se(4)	1.0211(2)	0.48156(7)	0.7940(2)	2.52(4)
S(1)	0.6284(7)	0.6743(2)	0.2582(7)	3.8(1)
S(2)	0.9448(6)	0.7056(2)	0.5864(7)	3.7(1)
S(3)	0.7297(7)	0.3515(2)	0.5603(7)	3.7(1)
S(4)	1.0412(6)	0.3778(2)	0.9145(7)	3.2(1)
S(5)	0.3379(6)	0.5665(2)	0.0107(6)	2.6(1)
S(6)	0.6486(6)	0.5420(2)	−0.1349(7)	2.9(1)
O(1)	0.333(2)	0.6913(5)	−0.124(2)	4.3(4)
O(2)	0.645(2)	0.6692(5)	−0.255(2)	3.8(4)
C(1)	0.844(2)	0.5494(6)	0.561(2)	2.0(4)
C(2)	0.742(2)	0.6338(7)	0.403(2)	2.6(4)
C(3)	0.872(2)	0.6478(7)	0.537(2)	2.7(4)
C(4)	0.629(3)	0.7214(8)	0.387(3)	5.0(6)
C(5)	0.777(3)	0.7454(7)	0.473(3)	4.6(6)
C(6)	0.867(2)	0.5043(7)	0.603(2)	1.8(4)
C(7)	0.820(2)	0.4071(6)	0.625(2)	1.6(4)
C(8)	0.948(2)	0.4172(6)	0.756(2)	1.8(4)
C(9)	0.845(3)	0.3108(7)	0.714(2)	3.1(5)
C(10)	0.886(3)	0.3317(7)	0.875(3)	4.0(5)
C(11)	0.427(2)	0.6049(7)	−0.081(2)	2.2(4)
C(12)	0.555(2)	0.5963(6)	−0.144(2)	1.9(4)
C(13)	0.414(2)	0.6558(7)	−0.129(3)	3.2(5)
C(14)	0.562(2)	0.6451(8)	−0.196(2)	3.1(5)
C(16)	0.178(1)	0.213(1)	0.351(1)	5.4(5)
C(17)	−0.071(1)	0.439(2)	0.767(2)	9.6(7)
C(18)	−0.038(1)	0.449(2)	0.655(1)	6.7(5)
C(19)	0.2770(9)	−0.068(1)	0.832(1)	3.5(4)
C(20)	0.7484(8)	−0.017(1)	1.084(1)	3.0(4)

(BETS)$_2$[Pd(dts)$_2$] ·2(1,1,2,2-TCE) (**2**)

Atom	x/a	y/b	z/c	B_{eq}/Å^2
Pd(1)	0.5000	0.0000	1.0000	2.40(3)
Se(1)	0.61278(8)	0.1504(1)	0.4452(1)	2.98(3)
Se(2)	0.38362(9)	0.1113(1)	0.6310(1)	3.63(4)
Se(3)	0.42642(8)	0.1570(1)	0.3566(1)	3.36(4)
Se(4)	0.55939(9)	0.1036(1)	0.7147(1)	3.48(4)
Cl(1)	0.0588(3)	0.4461(4)	0.6415(4)	6.6(1)
Cl(2)	−0.0745(3)	0.3281(4)	0.5845(5)	8.8(2)
Cl(3)	−0.0353(3)	0.3489(6)	0.8657(5)	11.4(2)
Cl(4)	−0.0387(3)	0.5706(5)	0.8235(6)	12.4(2)
S(1)	0.7753(2)	0.1685(3)	0.5280(3)	4.1(1)
S(2)	0.2618(2)	0.1678(4)	0.2806(4)	5.2(1)
S(3)	0.2159(2)	0.1113(3)	0.5692(4)	3.9(1)
S(4)	0.7121(2)	0.1283(3)	0.8243(3)	4.4(1)
S(5)	0.4376(2)	−0.1098(3)	0.8713(3)	3.3(1)
S(6)	0.6073(2)	−0.0929(3)	0.9669(3)	3.5(1)
O(2)	0.2448(6)	−0.1202(8)	0.7549(9)	5.1(3)
O(3)	0.8064(5)	−0.0544(8)	1.062(1)	5.2(3)
C(3)	0.5305(7)	0.131(1)	0.546(1)	2.9(3)
C(4)	0.4594(7)	0.132(1)	0.518(1)	2.5(3)
C(5)	0.3263(7)	0.149(1)	0.396(1)	3.3(3)
C(6)	0.3061(7)	0.126(1)	0.513(1)	3.0(4)
C(9)	0.3537(7)	−0.057(1)	0.877(1)	2.5(3)
C(10)	0.6662(8)	−0.025(1)	1.051(1)	3.1(4)
C(11)	0.8245(8)	0.104(1)	0.650(1)	4.5(4)
C(12)	0.8063(7)	0.150(1)	0.776(1)	4.0(4)
C(13)	0.6851(7)	0.151(1)	0.572(1)	2.8(3)
C(14)	0.6583 (8)	0.130(1)	0.688(1)	3.1(4)
C(15)	0.178(1)	0.217(1)	0.490(2)	6.4(5)

(BETS)[Au(dts)$_2$] (**4**)

Atom	x/a	y/b	z/c	B_{eq}/Å^2
Au(1)	0.0000	0.0000	0.0000	1.95(2)
Se(1)	0.3478(2)	−0.0914(1)	0.6700(3)	2.65(4)
Se(2)	0.5304(2)	−0.1486(1)	1.1295(3)	2.77(4)
S(1)	0.2272(6)	−0.3024(3)	0.4660(7)	3.3(1)
S(2)	0.4352(6)	−0.3662(3)	0.9718(7)	3.6(1)
S(3)	0.1537(5)	0.0806(3)	0.3461(7)	3.1(1)
S(4)	−0.0333(5)	0.1462(3)	−0.1528(7)	3.0(1)
O(1)	0.284(1)	0.3347(8)	0.566(2)	4.9(3)
O(2)	0.095(1)	0.4014(8)	0.082(2)	4.9(3)
C(1)	0.477(2)	−0.048(1)	0.960(2)	2.2(3)
C(2)	0.342(2)	−0.225(1)	0.711(2)	2.1(3)
C(3)	0.417(2)	−0.251(1)	0.897(2)	2.4(3)
C(4)	0.276(2)	−0.416(1)	0.528(3)	4.9(5)
C(5)	0.281(2)	−0.443(1)	0.753(3)	5.2(5)
C(6)	0.142(2)	0.195(1)	0.288(2)	2.3(3)
C(7)	0.071(2)	0.222(1)	0.074(3)	3.2(4)
C(8)	0.203(2)	0.298(1)	0.389(3)	4.4(5)
C(9)	0.119(2)	0.330(1)	0.162(3)	3.5(4)

(ET)$_2$[Pd(dts)$_2$] (**5**)

Atom	x/a	y/b	z/c	B_{eq}/Å^2
Pd(1)	0.0000	0.0000	0.5000	2.62(1)
S(1)	0.5642(1)	0.1619(2)	0.4252(1)	2.99(3)
S(2)	0.3360(1)	0.0934(2)	0.3714(1)	3.38(3)
S(3)	0.5591(1)	0.1389(2)	0.2206(1)	3.86(4)
S(4)	0.2823(1)	0.0523(2)	0.1561(1)	4.37(4)
S(5)	0.5872(1)	0.2197(2)	0.6540(1)	3.04(3)
S(6)	0.3591(1)	0.1474(2)	0.5953(1)	3.31(4)
S(7)	0.6294(1)	0.2712(2)	0.8671(1)	4.14(4)
S(8)	0.3598(1)	0.1895(2)	0.8004(1)	3.58(4)
S(9)	−0.1737(1)	0.0621(2)	0.3883(1)	3.28(4)
S(10)	0.0704(1)	0.0125(2)	0.3750(1)	3.48(4)
O(1)	−0.2944(4)	0.1202(5)	0.1106(3)	5.1(1)
O(2)	−0.0582(4)	0.0819(4)	0.0993(3)	4.8(1)
C(1)	0.4590(4)	0.1406(5)	0.4628(4)	2.8(1)
C(2)	0.4863(4)	0.1276(5)	0.2978(4)	2.7(1)
C(3)	0.3806(4)	0.0958(6)	0.2735(4)	2.8(1)
C(4)	0.4590(6)	0.0753(9)	0.1045(5)	6.8(2)
C(5)	0.3482(6)	0.093(1)	0.0772(5)	7.9(3)
C(6)	0.4679(4)	0.1647(5)	0.5611(4)	2.6(1)
C(7)	0.5358(4)	0.2215(6)	0.7489(4)	2.9(1)
C(8)	0.4313(5)	0.1862(6)	0.7226(4)	3.1(1)
C(9)	0.5451(5)	0.3064(6)	0.9355(4)	3.5(1)
C(10)	0.4253(5)	0.3225(6)	0.8726(4)	3.4(1)
C(11)	−0.1478(5)	0.0749(6)	0.2813(4)	3.0(1)
C(12)	−0.0476(5)	0.0544(6)	0.2769(4)	3.1(1)
C(13)	−0.2034(5)	0.0986(6)	0.1704(5)	3.6(2)
C(14)	−0.0913(5)	0.0787(6)	0.1654(5)	3.6(2)

Table 3. (Continued)

$(ET)_2[Pt(dts)_2]$(**6**)

Atom	x/a	y/b	z/c	B_{eq}/Å^2
Pt(1)	0.0000	0.0000	0.5000	2.61(3)
S(1)	0.5649(5)	0.1621(7)	0.4257(5)	3.0(2)
S(2)	0.3367(6)	0.0955(7)	0.3717(5)	3.5(2)
S(3)	0.5599(6)	0.1385(8)	0.2212(6)	3.9(2)
S(4)	0.2817(6)	0.0536(8)	0.1568(5)	4.5(2)
S(5)	0.5874(5)	0.2191(7)	0.6544(5)	3.2(2)
S(6)	0.3588(5)	0.1492(7)	0.5949(5)	3.3(2)
S(7)	0.6294(5)	0.2703(8)	0.8679(5)	4.1(2)
S(8)	0.3593(6)	0.1904(7)	0.8001(5)	3.8(2)
S(9)	−0.1721(5)	0.0579(7)	0.3871(5)	3.3(2)
S(10)	0.0694(5)	0.0144(8)	0.3750(5)	3.7(2)
O(1)	−0.296(2)	0.120(2)	0.101(1)	5.3(6)
O(2)	−0.056(2)	0.082(2)	0.099(2)	5.9(7)
C(1)	0.458(2)	0.137(2)	0.463(2)	2.6(6)
C(2)	0.486(2)	0.129(3)	0.298(2)	2.9(6)
C(3)	0.378(2)	0.092(3)	0.273(2)	3.4(7)
C(4)	0.460(3)	0.074(4)	0.104(3)	7(1)
C(5)	0.357(5)	0.092(5)	0.077(3)	11(1)
C(6)	0.472(2)	0.168(3)	0.560(2)	4.0(7)
C(7)	0.537(2)	0.223(2)	0.751(2)	2.7(6)
C(8)	0.432(2)	0.187(3)	0.719(2)	3.3(7)
C(9)	0.544(2)	0.306(3)	0.938(2)	4.1(7)
C(10)	0.427(2)	0.324(3)	0.873(2)	4.0(7)
C(11)	−0.147(2)	0.068(3)	0.284(2)	4.3(7)
C(12)	−0.050(2)	0.055(2)	0.275(2)	3.3(6)
C(13)	−0.205(2)	0.099(3)	0.174(2)	3.3(7)
C(14)	−0.092(3)	0.079(3)	0.168(2)	4.7(9)

$(ET)[Au(dts)_2]$(**7**)

Atom	x/a	y/b	z/c	B_{eq}/Å^2
Au(1)	0.0000	0.0000	0.5000	1.972(8)
Au(2)	0.5000	0.0000	0.0000	2.016(8)
S(1)	−0.1261(1)	0.1398(1)	1.0795(2)	2.58(4)
S(2)	0.1091(1)	0.0932(1)	1.0091(2)	2.63(4)
S(3)	−0.1688(1)	0.3547(1)	1.1625(3)	3.06(4)
S(4)	0.1164(1)	0.2987(1)	1.0761(2)	2.94(4)
S(5)	0.6084(1)	0.0888(1)	0.6756(2)	2.65(4)
S(6)	0.3738(1)	0.1439(1)	0.4086(2)	2.61(4)
S(7)	0.6181(2)	0.2917(1)	0.7812(3)	3.21(4)
S(8)	0.3404(2)	0.3586(1)	0.4460(2)	3.00(4)
S(9)	−0.1259(1)	−0.0929(1)	0.4894(2)	2.68(4)
S(10)	0.1532(1)	−0.1408(1)	0.4247(2)	2.90(4)
S(11)	0.6373(1)	0.0753(1)	0.1996(2)	2.60(4)
S(12)	0.3579(1)	0.1519(1)	−0.1029(2)	2.74(4)
O(1)	−0.0935(5)	−0.3579(4)	0.3846(7)	4.8(1)
O(2)	0.1785(4)	−0.4074(4)	0.3231(7)	4.2(1)
O(3)	0.6259(4)	0.3350(3)	0.3140(6)	3.7(1)
O(4)	0.3585(5)	0.4114(4)	0.0176(6)	4.3(1)
C(1)	−0.0031(6)	0.0491(5)	1.0203(8)	2.0(1)
C(2)	−0.0719(5)	0.2390(5)	1.1000(8)	2.1(1)
C(3)	0.0367(5)	0.2171(5)	1.0680(8)	1.9(1)
C(4)	−0.1014(7)	0.4376(5)	1.125(1)	3.4(2)
C(5)	0.0367(6)	0.4064(5)	1.193(1)	3.1(2)
C(6)	0.4958(6)	0.0492(5)	0.518(1)	2.3(1)
C(7)	0.5388(5)	0.2139(4)	0.6429(8)	2.0(1)
C(8)	0.4307(5)	0.2411(5)	0.5151(8)	2.2(1)
C(9)	0.5320(7)	0.4111(5)	0.694(1)	3.9(2)
C(10)	0.3959(7)	0.4334(6)	0.633(1)	3.5(2)
C(11)	−0.0305(6)	−0.2068(5)	0.4311(8)	2.2(1)
C(12)	0.0824(5)	−0.2259(5)	0.4053(8)	2.3(1)
C(13)	−0.0267(7)	−0.3128(5)	0.3900(9)	3.2(2)
C(14)	0.1017(6)	−0.3352(5)	0.3639(9)	3.0(2)
C(15)	0.5498(5)	0.1953(5)	0.1521(8)	2.3(1)
C(16)	0.4393(5)	0.2263(5)	0.0323(8)	2.2(1)
C(17)	0.5559(6)	0.2969(5)	0.2079(9)	2.6(1)
C(18)	0.4298(6)	0.3335(5)	0.0713(9)	2.7(2)

$B_{eq} = \frac{8}{3}\pi^2(U_{11}(aa^*)^2+U_{22}(bb^*)^2+U_{33}(cc^*)^2+2U_{12}aa^*bb^*\cos\gamma+2U_{13}aa^*cc^*\cos\beta+2U_{23}bb^*cc^*\cos\alpha)$.

ture determination, the quadrilateral of cyclobutene of bis-(dithiosquarato)metalate anions are not regular squares, but trapeziums. In other words, their C1–C2 bond lengths are shorter than their C3–C4 bond lengths (Fig. 4), which suggest that bis(dithiosquarato)metalate anions favor the mesomeric form I and to a lesser extent forms II and III.

Crystal Structures. From the results of single-crystal X-ray structure determinations, the donor : anion ratio of salts **1**, **2**, **5**, and **6** are 2 : 1, and that of salts **4** and **7** are 1 : 1. The stacking pattern of these salts is a kind of mixed stack. In the case of 2 : 1 salts, a dimer of the donor molecules and the $[M(dts)_2]$ molecule stack alternatively. As for salts **1** and **2**, the molecular plane of an anion is almost perpendicular to the molecular planes of the donors, and as for salts **5** and **6**, the molecular long axes of the anions and the donors are not parallel, but slip each other. On the other hand, in the case of 1 : 1 salts a donor molecule and a $[Au(dts)_2]$ molecule stack alternatively and pile up their molecular planes. Salts **5** and **6** are completely isomorphous; hereafter, salt **5** is mainly discussed in the following section. The sums of the van der Waals radii of the molecular contacts are S···S = 3.70 Å, S···Se = 3.85 Å, Se···Se = 4.00 Å, and S···O = 3.25 Å. In

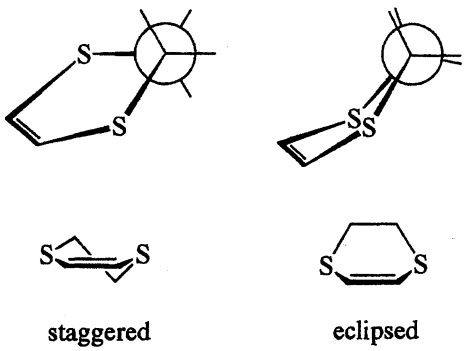

Fig. 3. Schematic drawings of the conformation of the terminal ethylene group. Only one of the terminal six-membered ring of BETS and ET are drawn.

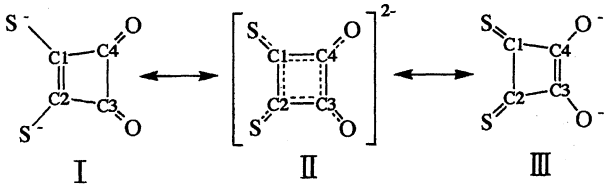

Fig. 4. Possible resonance forms of dithiosquarate ligand.

Table 4. Selected Bond Lengths (Å) and Bond Angles (°) of Cation Radical Salts **1**, **2**, **4**, **5**, **6**, and **7**

(BETS)$_2$[Pd(dts)$_2$] (**1**)

Bond length (Å)			
Pd(1)–S(5)	2.329(5)	S(4)–C(8)	1.77(2)
Pd(1)–S(6)	2.324(6)	S(4)–C(10)	1.79(2)
Se(1)–C(1)	1.86(2)	S(5)–C(11)	1.67(2)
Se(1)–C(2)	1.85(2)	S(6)–C(12)	1.70(2)
Se(2)–C(1)	1.90(2)	O(1)–C(13)	1.21(2)
Se(2)–C(3)	1.85(2)	O(2)–C(14)	1.21(2)
Se(3)–C(6)	1.89(2)	C(1)–C(6)	1.31(2)
Se(3)–C(7)	1.86(2)	C(2)–C(3)	1.40(2)
Se(4)–C(6)	1.90(2)	C(4)–C(5)	1.42(3)
Se(4)–C(8)	1.89(2)	C(7)–C(8)	1.35(2)
S(1)–C(2)	1.75(2)	C(9)–C(10)	1.49(3)
S(1)–C(4)	1.74(2)	C(11)–C(12)	1.39(2)
S(2)–C(3)	1.73(2)	C(11)–C(13)	1.47(3)
S(2)–C(5)	1.84(2)	C(12)–C(14)	1.45(3)
S(3)–C(7)	1.74(2)	C(13)–C(14)	1.59(3)
S(3)–C(9)	1.81(2)		
Bond angle (°)			
S(5)–Pd(1)–S(6)	92.8(2)	Pd(1)–S(6)–C(13)	98.4(7)
S(5)–Pd(1)–S(6)*	87.2(2)	S(5)–C(11)–C(12)	128(1)
Pd(1)–S(5)–C(11)	96.9(7)	S(6)–C(12)–C(11)	123(1)

(BETS)$_2$[Pd(dts)$_2$]·2(1,1,2,2-TCE) (**2**)

Bond length (Å)			
Pd(1)–S(5)	2.329(4)	S(3)–C(7)	1.71(1)
Pd(1)–S(6)	2.325(4)	S(3)–C(9)	1.77(1)
Se(1)–C(1)	1.88(1)	S(4)–C(8)	1.76(1)
Se(1)–C(2)	1.86(1)	S(4)–C(10)	1.75(1)
Se(2)–C(1)	1.85(1)	S(5)–C(11)	1.67(1)
Se(2)–C(3)	1.89(1)	S(6)–C(13)	1.68(1)
Se(3)–C(6)	1.86(1)	O(1)–C(12)	1.18(2)
Se(3)–C(7)	1.90(1)	O(2)–C(14)	1.24(2)
Se(4)–C(6)	1.95(1)	C(1)–C(6)	1.32(2)
Se(4)–C(8)	1.84(1)	C(2)–C(3)	1.35(2)
Cl(1)–C(15)	1.91(2)	C(4)–C(5)	1.47(2)
Cl(2)–C(15)	1.73(2)	C(7)–C(8)	1.37(2)
Cl(3)–C(16)	1.71(2)	C(9)–C(10)	1.53(2)
Cl(4)–C(16)	1.95(2)	C(11)–C(12)	1.51(2)
S(1)–C(2)	1.74(1)	C(11)–C(13)	1.39(2)
S(1)–C(4)	1.78(2)	C(12)–C(14)	1.53(2)
S(2)–C(3)	1.74(1)	C(13)–C(14)	1.46(2)
S(2)–C(5)	1.76(2)	C(15)–C(16)	1.35(2)
Bond angle (°)			
S(5)–Pd(1)–S(6)	87.9(1)	Pd(1)–S(6)–C(13)	98.1(4)
S(5)–Pd(1)–S(6)*	92.1(1)	S(5)–C(11)–C(13)*	125(1)
Pd(1)–S(5)–C(1)	98.2(5)	S(6)–C(13)–C(11)*	125.6(10)

(BETS)[Au(dts)$_2$] (**4**)

Bond length (Å)			
Au(1)–S(3)	2.340(4)	S(4)–C(7)	1.67(1)
Au(1)–S(3)*	2.343(4)	O(1)–C(8)	1.18(2)
Se(1)–C(1)	1.88(1)	O(2)–C(9)	1.17(2)
Se(1)–C(2)	1.90(1)	C(1)–C(1)	1.35(3)
Se(2)–C(1)	1.88(1)	C(2)–C(3)	1.29(2)
Se(2)–C(3)	1.92(1)	C(4)–C(5)	1.39(2)
S(1)–C(2)	1.78(1)	C(6)–C(7)	1.43(2)
S(1)–C(4)	1.79(2)	C(6)–C(8)	1.48(2)
S(2)–C(3)	1.73(1)	C(7)–C(9)	1.53(2)
S(2)–C(5)	1.79(2)	C(8)–C(9)	1.56(2)
S(3)–C(6)	1.69(1)		
Bond angle (°)			
S(3)–Au(1)–S(4)	93.1(1)	Au(1)–S(4)–C(7)	97.2(6)
S(3)–Au(1)–S(4)*	86.9(1)	S(3)–C(6)–C(7)	124(1)
Au(1)–S(3)–C(6)	97.6(5)	S(4)–C(7)–C(6)	127(1)

(ET)$_2$[Pd(dts)$_2$] (**5**)

Bond length (Å)			
Pd(1)–S(9)	2.331(3)	S(8)–C(8)	1.737(6)
Pd(1)–S(10)	2.342(2)	S(8)–C(10)	1.823(7)
S(1)–C(1)	1.709(6)	S(9)–C(11)	1.712(6)
S(1)–C(2)	1.746(5)	S(10)–C(12)	1.703(6)
S(2)–C(1)	1.720(6)	O(1)–C(13)	1.195(7)
S(2)–C(3)	1.734(6)	O(2)–C(14)	1.197(7)
S(3)–C(2)	1.748(6)	C(1)–C(6)	1.396(7)
S(3)–C(4)	1.810(7)	C(2)–C(3)	1.355(8)
S(4)–C(3)	1.738(5)	C(4)–C(5)	1.38(1)
S(4)–C(5)	1.749(9)	C(7)–C(8)	1.348(8)
S(5)–C(6)	1.726(6)	C(9)–C(10)	1.496(8)
S(5)–C(7)	1.754(6)	C(11)–C(12)	1.382(8)
S(6)–C(6)	1.720(6)	C(11)–C(13)	1.486(8)
S(6)–C(8)	1.745(6)	C(12)–C(14)	1.493(8)
S(7)–C(7)	1.746(6)	C(13)–C(14)	1.541(9)
S(7)–C(9)	1.809(7)		
Bond angle (°)			
S(9)–Pd(1)–S(10)	92.74(10)	Pd(1)–S(10)–C(12)	97.5(2)
S(9)–Pd(1)–S(10)*	87.26(10)	S(9)–C(11)–C(12)	125.1(4)
Pd(1)–S(9)–C(11)	98.1(2)	S(10)–C(12)–C(11)	126.6(5)

(ET)$_2$[Pt(dts)$_2$] (**6**)

Bond length (Å)			
Pt(1)–S(9)	2.327(6)	S(8)–C(8)	1.71(3)
Pt(1)–S(10)	2.297(7)	S(8)–C(10)	1.84(3)
S(1)–C(1)	1.66(3)	S(9)–C(11)	1.68(3)
Se(1)–C(2)	1.72(3)	S(10)–C(12)	1.66(3)
S(2)–C(1)	1.75(2)	O(1)–C(13)	1.27(4)
S(2)–C(3)	1.73(3)	O(2)–C(14)	1.21(3)
S(3)–C(2)	1.70(3)	C(1)–C(6)	1.38(4)
S(3)–C(4)	1.84(4)	C(2)–C(3)	1.39(3)
S(4)–C(3)	1.77(3)	C(4)–C(5)	1.31(6)
S(4)–C(5)	1.81(4)	C(7)–C(8)	1.35(3)
S(5)–C(6)	1.79(3)	C(9)–C(10)	1.50(4)
S(5)–C(7)	1.69(3)	C(11)–C(12)	1.37(4)
S(6)–C(6)	1.68(3)	C(11)–C(13)	1.45(4)
S(6)–C(8)	1.78(2)	C(12)–C(14)	1.50(4)
S(7)–C(7)	1.79(3)	C(13)–C(14)	1.55(5)
S(7)–C(9)	1.82(3)		
Bond angle (°)			
S(9)–Pt(1)–S(10)	91.2(2)	Pt(1)–S(10)–C(12)	99(1)
S(9)–Pt(1)–S(10)*	88.8(2)	S(9)–C(11)–C(12)	124(2)
Pt(1)–S(9)–C(11)	98.6(9)	S(10)–C(12)–C(11)	126(2)

Table 4. (Continued)

(ET)[Au(dts)$_2$] (**7**)

Bond length (Å)				S(6)–C(8)	1.747(6)	C(11)–C(13)	1.492(9)
Au(1)–S(9)	2.344(2)	S(12)–C(16)	1.720(6)	S(7)–C(7)	1.749(6)	C(12)–C(14)	1.497(9)
Au(1)–S(10)	2.343(2)	O(1)–C(13)	1.197(8)	S(7)–C(9)	1.796(8)	C(13)–C(14)	1.548(10)
Au(2)–S(11)	2.342(2)	O(2)–C(14)	1.196(8)	S(8)–C(8)	1.733(6)	C(15)–C(16)	1.351(8)
Au(2)–S(12)	2.343(2)	O(3)–C(17)	1.206(7)	S(8)–C(10)	1.783(8)	C(15)–C(17)	1.473(9)
S(1)–C(1)	1.727(7)	O(4)–C(18)	1.199(8)	C(9)–C(11)	1.718(6)	C(16)–C(18)	1.490(9)
S(1)–C(2)	1.742(7)	C(1)–C(1)*	1.37(1)	S(10)–C(12)	1.697(7)	C(17)–C(18)	1.542(9)
S(2)–C(1)	1.732(7)	C(2)–C(3)	1.339(8)	S(11)–C(15)	1.710(6)		
S(2)–C(3)	1.736(6)	C(4)–C(5)	1.503(9)				
S(3)–C(2)	1.753(6)	C(6)–C(6)*	1.37(1)	Bond angle (°)			
S(3)–C(4)	1.791(8)	C(7)–C(8)	1.359(8)	S(9)–Au(1)–S(10)	92.88(6)	Au(2)–S(11)–C(15)	96.3(2)
S(4)–C(3)	1.755(7)	S(8)–C(8)	1.733(6)	S(9)–Au(1)–S(10)*	87.12(6)	Au(2)–S(12)–C(16)	96.4(2)
S(4)–C(5)	1.790(7)	S(8)–C(10)	1.783(8)	S(11)–Au(2)–S(12)	93.46(6)	S(9)–C(11)–C(12)	126.5(5)
S(5)–C(6)	1.731(7)	C(9)–C(11)	1.718(6)	S(11)–Au(2)–S(12)*	86.54(6)	S(10)–C(12)–C(11)	126.1(5)
S(5)–C(7)	1.725(6)	C(9)–C(10)	1.49(1)	Au(1)–S(9)–C(11)	96.8(2)	S(11)–C(15)–C(17)	138.7(5)
S(6)–C(6)	1.725(7)	C(11)–C(12)	1.373(9)	Au(1)–S(10)–C(12)	97.6(2)	S(12)–C(16)–C(15)	126.5(5)

Figs. 5, 6, 7, 8, and 9, the broken lines represent the short contacts within the sum of the van der Waals radii. The C–H···O hydrogen bonds are discussed in the next section.

(BETS)$_2$[Pd(dts)$_2$] (1) and (BETS)$_2$[Pd(dts)$_2$]·2(1,1,2,2-TCE) (2). In spite of their quite different cell parameters, these two salts show a similar molecular arrangement of the stacking patterns of the BETS dimers and [Pd(dts)$_2$] anions. In the case of salt **1**, the crystal structure is shown in Fig. 5. The BETS dimer and [Pd(dts)$_2$] anions stack along the [10$\bar{1}$] direction with their long molecular axis toward almost the [010] direction (Figs. 5a and 5b). The intermolecular short contacts within the sum of the van der Waals radii are shown

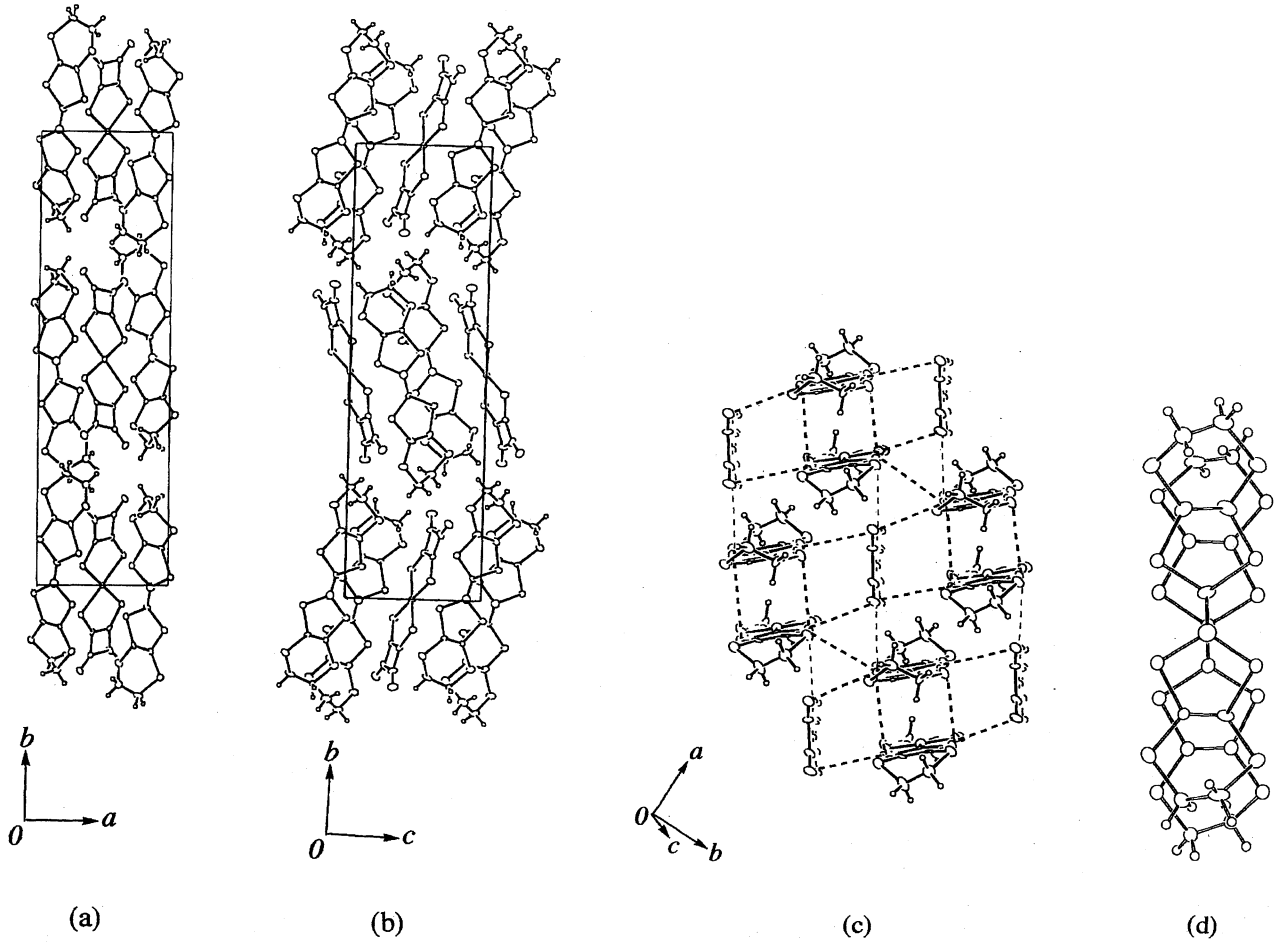

Fig. 5. Crystal structure of (BETS)$_2$[Pd(dts)$_2$] (**1**). (a) View of the unit cell along the *c* axis, (b) along the *a* axis. (c) View of the stacked pattern along the molecular long axis. In Figs. 5, 6, 7, 8, and 9, the broken lines represent the short contacts within the sum of the van der Waals radii. (d) Mode of the overlap of the dimer of BETS molecules.

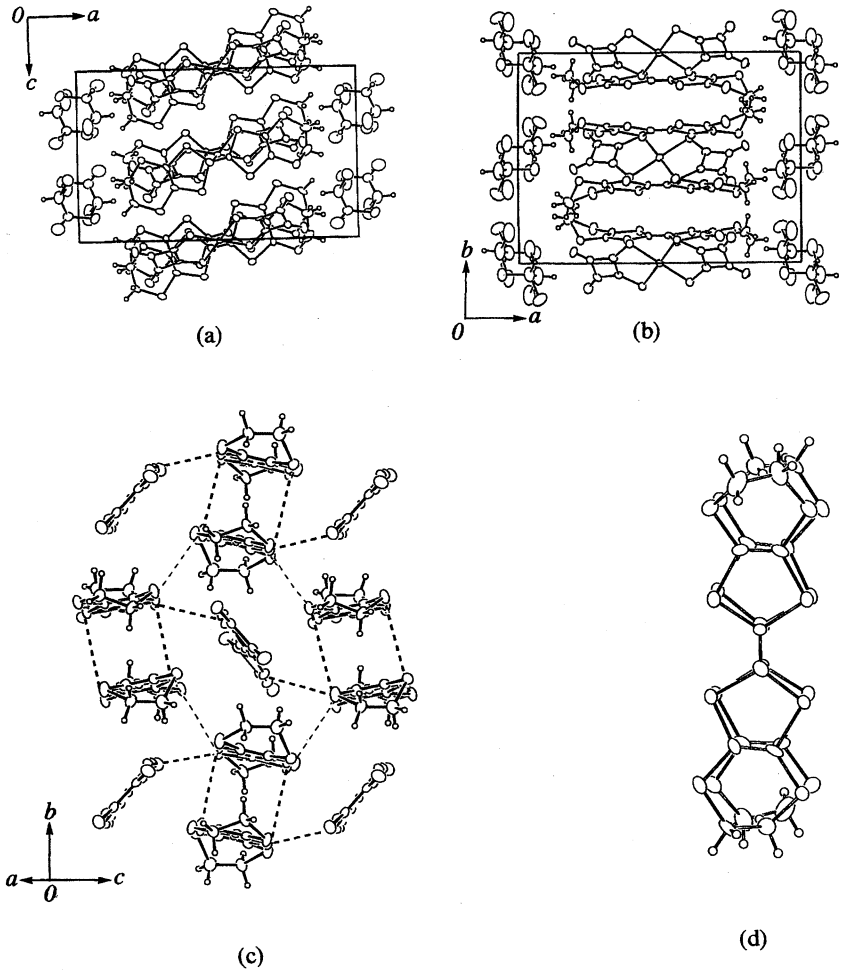

Fig. 6. Crystal structure of (BETS)$_2$[Pd(dts)$_2$]·2(1,1,2,2-TCE) (**2**). (a) View of the unit cell along the *b* axis, (b) along the *c* axis. (c) View of the stacked pattern along the molecular long axis. (d) Mode of the overlap of the dimer of BETS molecules.

in Fig. 5c. The Se···Se distances in the intradimer of BETS are very short, 3.65—3.67 Å. The dihedral angle between the molecular plane of the BETS dimer and [Pd(dts)$_2$] anion is 83.2°, almost vertical. The structure will also be considered such that six BETS molecules form hexagonal donor networks and the anions occupy the open space. The [Pd(dts)$_2$] anion is surrounded by six BETS molecules, and intermolecular short contacts exist between each of the six BETS and [Pd(dts)$_2$] anion. The mode of the overlap of the BETS dimer is shown in Fig. 5d. Since the mode is a "bond over ring" type, the interplanar distance within a BETS dimer is very short (3.48 Å); thus, these BETS molecules are strongly dimerized.

In the case of salt **2**, the crystal structure is shown in Fig. 6, and salt **2** includes the organic solvent 1,1,2,2-tetrachloroethane (1,1,2,2-TCE) for crystallization. The BETS dimer and [Pd(dts)$_2$] anion stack along the [010] direction with their long molecular axis toward almost the [100] direction (Figs. 6a and 6b). Although the Se···Se distances in intradimer of BETS are 3.60—3.62 Å, shorter than those of the salt **1**, the interplanar distance within a BETS dimer is longer (3.66 Å), because the mode of the overlap is a "bond over bond" type (Fig. 6d). In Fig. 6c, the dihedral angle between the molecular plane of the BETS and [Pd(dts)$_2$] anion is about 60°, which is much smaller than that of salt **1**. [Pd(dts)$_2$] anions are also surrounded by six BETS molecules. However, compared with salt **1**, the number of contacts within the van der Waals radii is decreased between chalcogens of the BETS and [Pd(dts)$_2$] anion along the [001] direction.

(ET)$_2$[Pd(dts)$_2$] (5) and (ET)$_2$[Pt(dts)$_2$] (6). These salts are completely isomorphous. Since salt **6** has already been reported by C. Bellitto et al.,[24] here salt **5** is mainly discussed. As shown in Figs. 7a and 7b, the ET dimer and [Pd(dts)$_2$] anion stack alternatively and make columns along the [010] direction with their long molecular axis toward almost the [001] direction. The molecular arrangements of (ET)$_2$[Pd(dts)$_2$] ($x\approx0.0$) and (ET)$_2$[Pd(dts)$_2$] ($x\approx0.5$) are shown as the unshaded column and the shaded column. In the same column, the ET and [Pd(dts)$_2$] anion, and the ET dimers are parallel. However, between the shaded columns and the unshaded columns, these neighboring molecules arrange with a 142° dihedral angle of their molecular planes, and their molecular long axes are not parallel, but crossing. In short, the shaded columns and the unshaded columns form the crossing column. Thus, the shaded column and the un-

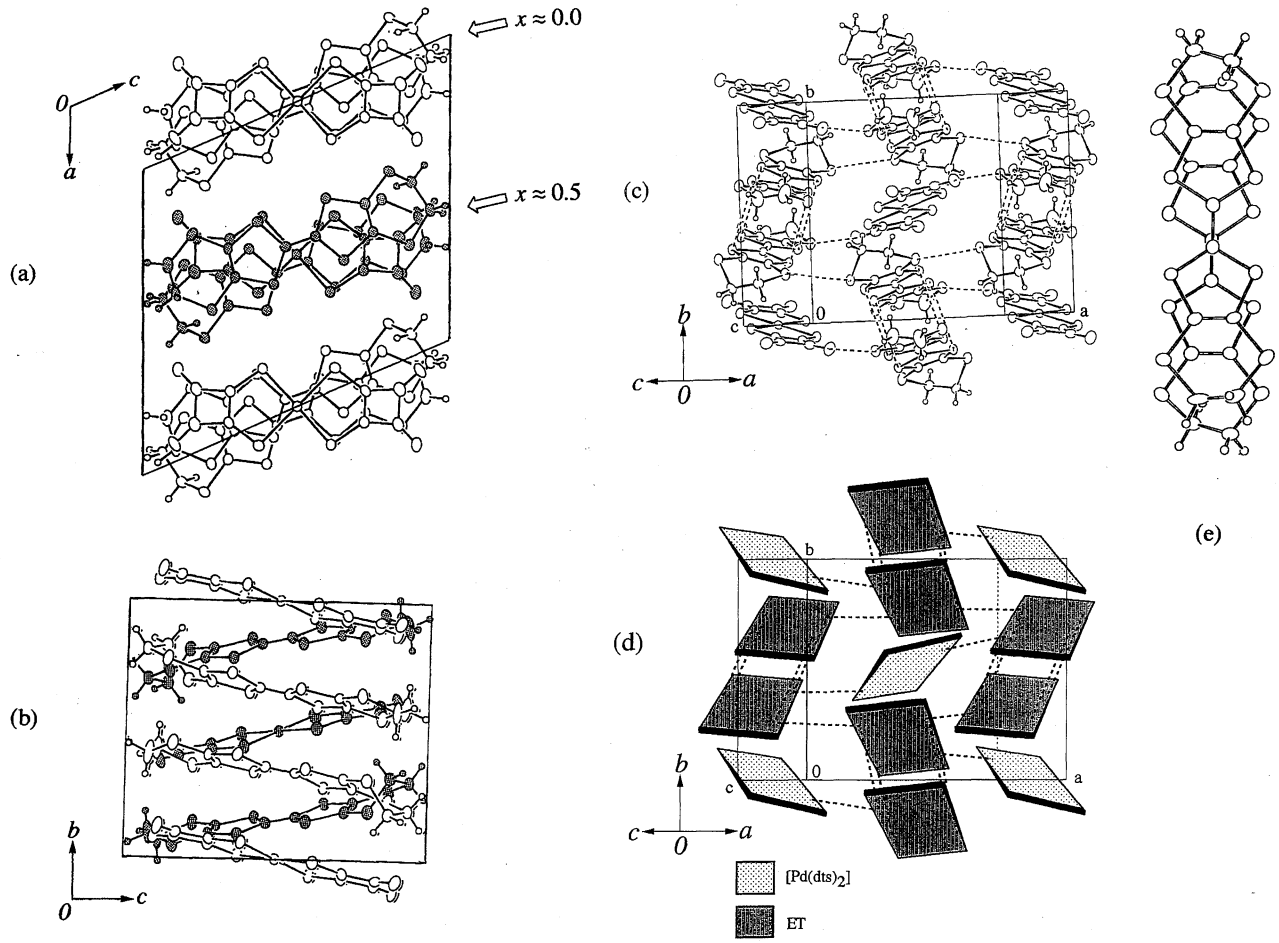

Fig. 7. Crystal structure of $(ET)_2[Pd(dts)_2]$ (**5**) and $(ET)_2[Pt(dts)_2]$ (**6**). (a) View of the unit cell along the *b* axis, (b) along the *a* axis. The molecular arrangement is shown as the unshaded $(ET)_2[Pd(dts)_2]$ column ($x\approx0.0$) and the shaded $(ET)_2[Pd(dts)_2]$column ($x\approx0.5$). (c) View of the molecular arrangement along the molecular long axis. (d) Schematic figure of Fig. 7c. (e) Mode of the overlap of the dimer of ET molecules.

shaded column make zigzag contacts viewed along the [100] direction (Fig. 7b).

The S···S distances within an intradimer of ET are 3.65—3.71 Å, and the mode of the overlap of the ET dimer is a "bond over ring" type (Fig. 7e). Thus, the interplanar distance within an ET dimer is very short (3.45 Å). On the other hand, the interplanar distance between the ET and $[Pd(dts)_2]$ anion in the same column is 3.55 Å, not very long. However, the molecular long axes of the ET and $[Pd(dts)_2]$ anion slip past each other (Fig. 7a) and the S···S distances between them are out of the sum of the van der Waals radii (3.81—4.52 Å). Therefore, in this salt, the intermolecular contacts within the sum of the van der Waals radii are very complex, as shown in Fig. 7c. The $[Pd(dts)_2]$ anion is surrounded by six ET molecules, and has short contacts with ET dimers in the transverse direction. The schematic molecular arrangements of simplified ET and anion molecules are shown in Fig. 7d.

The R and R_w values of salt **6** are not so good because of the poor quality of our crystal. More accurate bond lengths of salt **6** are discussed in the paper of C. Bellitto et al.[24]

(BETS)[Au(dts)$_2$] (4) and (ET)[Au(dts)$_2$] (7). The donor : anion ratio of salts **4** and **7** is 1 : 1, which is different from that of other 2 : 1 salts. The crystal structure of salt **4** is shown in Figs. 8a and 8b. The BETS and $[Au(dts)_2]$ anion stack alternatively along the [100] direction with their long molecular axis toward the [011] direction. The molecular planes of the BETS and $[Au(dts)_2]$ anion are almost parallel. The characteristic stacking pattern of salt **4** is shown in Fig. 8c. Many short contacts are found in the direction of **A** (3.72 Å for the shortest Se···Se contact), **B** (3.64 Å for Se···S, 3.25 Å for S···O), **C** (3.66 Å for S···S). However, along the [100] direction of molecular stacking, the distances between the Se···S and S···S contacts are more than 4.0 Å, which are longer than the sum of the van der Waals radii. The distance between the molecular planes of the BETS and $[Au(dts)_2]$ anion is 3.63 Å. A top view of the projection of the $[Au(dts)_2]$ anion on the molecular plane of BETS is shown in Fig. 8d. The BETS and $[Au(dts)_2]$ anion slip along the direction of their short molecular axis, and that mode of overlap causes an increases in the distances between the chalcogens in the stacking direction. The strong contacts exist along the [001] direction but not along the stacking direction. Therefore, such a concept as column structure loses its significance for salt **4**. The molecular arrangement of salt **4** will be con-

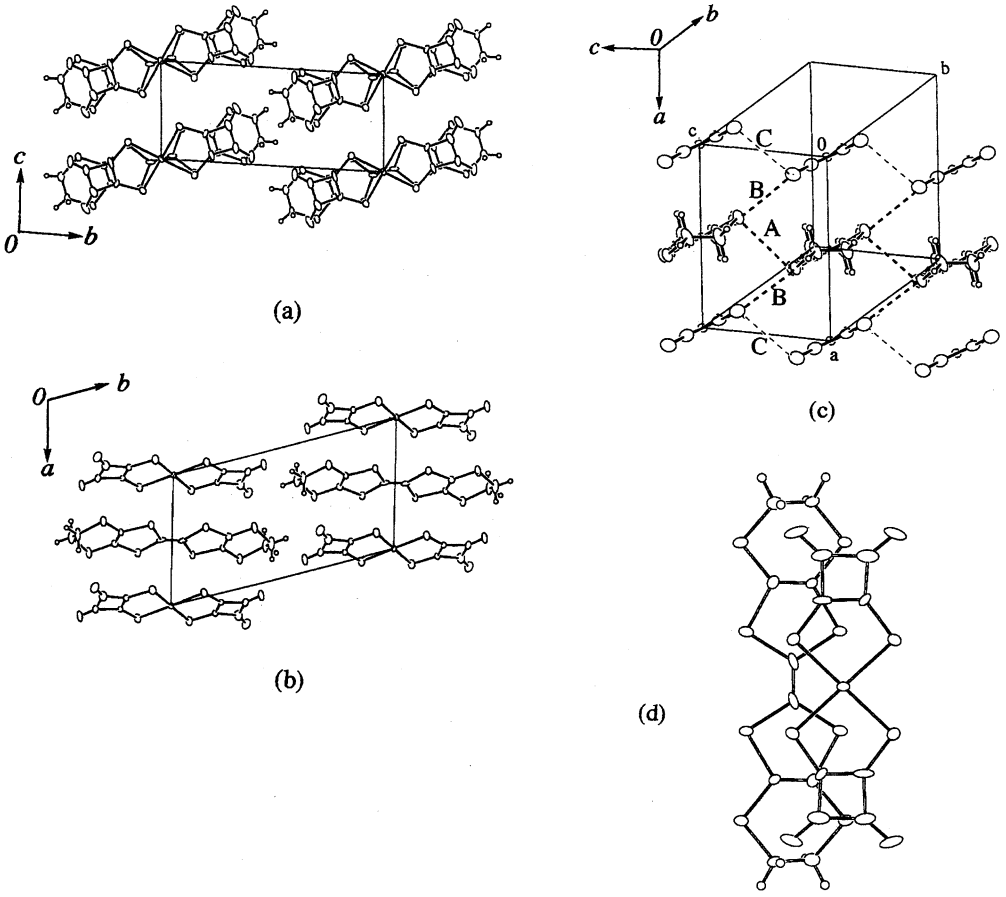

Fig. 8. Crystal structure of (BETS)[Au(dts)$_2$] (**4**). (a) View of the unit cell along the *a* axis, (b) along the *c* axis. (c) View of the stacked pattern along the molecular long axis. (d) Mode of the overlap of the dimer of BETS molecule and [Au(dts)$_2$] molecule.

sidered to be such that BETS forms a one-dimensional BETS chain along the [001] direction, which has short side-by-side contacts.

On the other hand, salt **7** has two pairs of ET and [Au(dts)$_2$] anion in its unit cell, which are crystallographically independent ($x\approx0$ and $x\approx0.5$). The ET and [Au(dts)$_2$] anion stack alternatively along the [001] direction with their long molecular axis toward the [010] direction (Figs. 9a and 9b). The molecular planes of the ET and [Au(dts)$_2$] anion are parallel in the same column. However, since the dihedral angle of the molecular planes between neighboring columns is about 55° (Fig. 9c), the stacking pattern of salt **7** is different from that of salt **4**. The top views of the projection of the [Au(dts)$_2$] anion on the plane of the ET molecule are almost the same in both columns (Fig. 9d). The distance between the molecular plane of the ET and [Au(dts)$_2$] anion is 3.62 Å in the $x\approx0$ column and 3.53 Å in the $x\approx0.5$ column. Therefore, there exist comparatively short contacts between the molecular stacking direction in the $x\approx0.5$ column, while the distances between the chalcogens are more than 4.0 Å for S···S in the $x\approx0$ column. There are short contacts within the sum of the van der Waals radii between the neighboring molecules, such as **D** (3.51 Å for the shortest S···S contacts, 3.23 Å for S···O), **E** (3.55 Å for S···S), **F** (3.54 Å for S···S), **G** (3.51 Å for S···S), and **H** (3.67 Å for S···S).

Structure of 3 Salt. (BETS)$_x$[Pd(dts)$_2$] ($x\approx5.0$) (**3**) salt is a metallic conductor and is obtained as large thin crystals (5.0×3.5×0.1 mm). The lattice parameters of salt **3** are given in Table 2. However, its crystal structure has not been determined satisfactorily, and only the arrangement of the BETS molecules has been determined. The BETS molecules pile up along the *b*-axis direction, and there are disorders in the arrangements of the anions. An X-ray oscillation photograph shows that the five-fold superstructure streaks along the $\mathbf{b}^*$-axis direction. According to an electron-probe microanalysis, the 5 : 1 of the donor : anion ratio is supported. From the Weissenberg X-ray photographs of salt **3**, although only Bragg spots are observed in the $k=0$ layer, in the $k=1$ layer Bragg spots are observed only on $h=2n+1$ and streaks appear on $h=2n$. Furthermore, in the $k=2$ layer, spots and streaks appear on $h=2n$ and on $h=2n+1$, respectively. These complicated X-ray photograph pattern are related to the disorder of the anions.

A similar cation radical salts, ET and $[Pd(dto)_2]^{2-}$ anion (dto=dithiooxalate), was reported to be a metallic conductor, whose donor : anion ratio is 4 : 1. The charge on ET was +0.5 and ET molecules constructed the two-dimensional sheet of donor layers, which were sandwiched by the anion layers.[25] From the arrangement of the BETS molecules and the unit cell volume of salt **3**, there is not sufficient space for anions to stack with their molecular planes piling up. Therefore, the structure of salt **3** seems to be similar to (ET)$_4$[Pd(dto)$_2$]. The

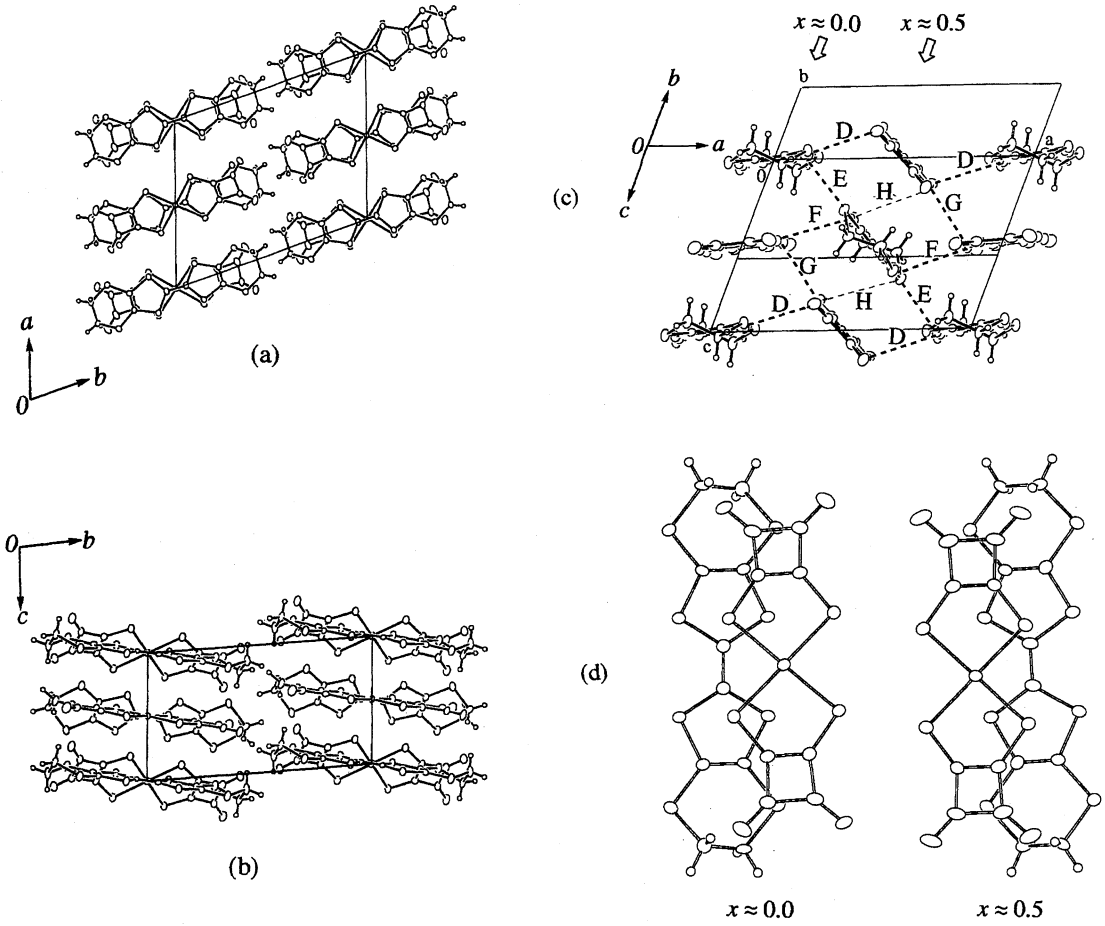

Fig. 9. Crystal structure of (ET)[Au(dts)$_2$] (**7**). (a) View of the unit cell along the *c* axis, (b) along the *a* axis. (c) View of the stacked pattern along the molecular long axis. (d) Mode of the overlap of the dimer of ET molecule and [Au(dts)$_2$] molecule.

[Pd(dts)$_2$] anion is larger than the [Pd(dto)$_2$] anion, which explains the 5 : 1 donor : anion ratio of salt **3**.

C–H···O Hydrogen Bonds. The hydrogen bonds, such as O–H···O and N–H···O, are sufficiently strong for determining the molecular arrangements and conformations. In these salts containing bis(dithiosquarato)metalate anions, since there are ethylene groups of donors and C=O groups of anions in the crystals, C–H···O hydrogen bonds are expected. The bond lengths, angles, and interactions of the C–H···O hydrogen bonds are discussed in many compounds,[26,27] and it becomes more and more important to consider the C–H···O hydrogen bonds for understanding the molecular arrangements. In these salts, there are many short C–H···O contacts which can be considered to be C–H···O hydrogen bonds. In our cation-radical salts, the hydrogen atoms are calculated as the terminal hydrocarbon with an sp^3 conformation. In Fig. 10, the selected C–H···O hydrogen bonds of salts **2**, **4**, and **7** are shown as dotted lines. In particular, one of the terminal ethylene groups of the BETS molecule of salt **2** markedly bends toward the carboxyl group of [Pd(dts)$_2$], and has an eclipsed conformation, although there are no special steric hindrances around the terminal ethylene groups of BETS (Fig. 10a). It is due to the C–H···O hydrogen bonds. On the other hand, the terminal ethylene groups of donors in salts **4** and **7** take a staggered conformation (Figs. 8c and 9c). Because their terminal ethylene groups have no interaction with the [Au(dts)$_2$] anions positioned at the upper or lower sides of their molecular plane, they have C–H···O hydrogen bonds with the [Au(dts)$_2$] anions along the directions, such as **I**, **J**, **K**, **L**, **M**, **N**, **O**, and **P** in Figs. 10b and 10c.

The conformation of the terminal ethylene groups of the other salts (**1**, **5**, and **6**) can be explained by C–H···O bonds. The donor : anion ratio 2 : 1 salts prefer an eclipsed conformation while the 1 : 1 salts prefer a staggered conformation. This is because in the former, since one of the donor molecules of the dimer is sandwiched between the other donor and an anion molecule, its ethylene groups bend toward the anion. In the latter, since a donor molecule is sandwiched between anions, the ethylene groups are balanced on its donor molecular plane.

Electrical Resistivity. The resistivity at room temperature is listed in Table 5. Salts **1**, **2**, **4**, **5**, **6**, and **7** show high resistivities ($\rho_{rt} = 10^3$—10^4 Ω cm). Their temperature dependences of the electrical resistivities show a semiconducting behavior. The activation energies of salts **5** and **6** are not tabulated, because their measurements are performed in the form of a pellet. Salt **3** shows low resistivity at room temperature ($\rho_{rt} = 0.025$ Ω cm), and its temperature dependence of the electrical resistivity is metallic down to 4 K and $\rho/\rho_{rt} = 0.1$ (Fig. 11). Compared with the other semicon-

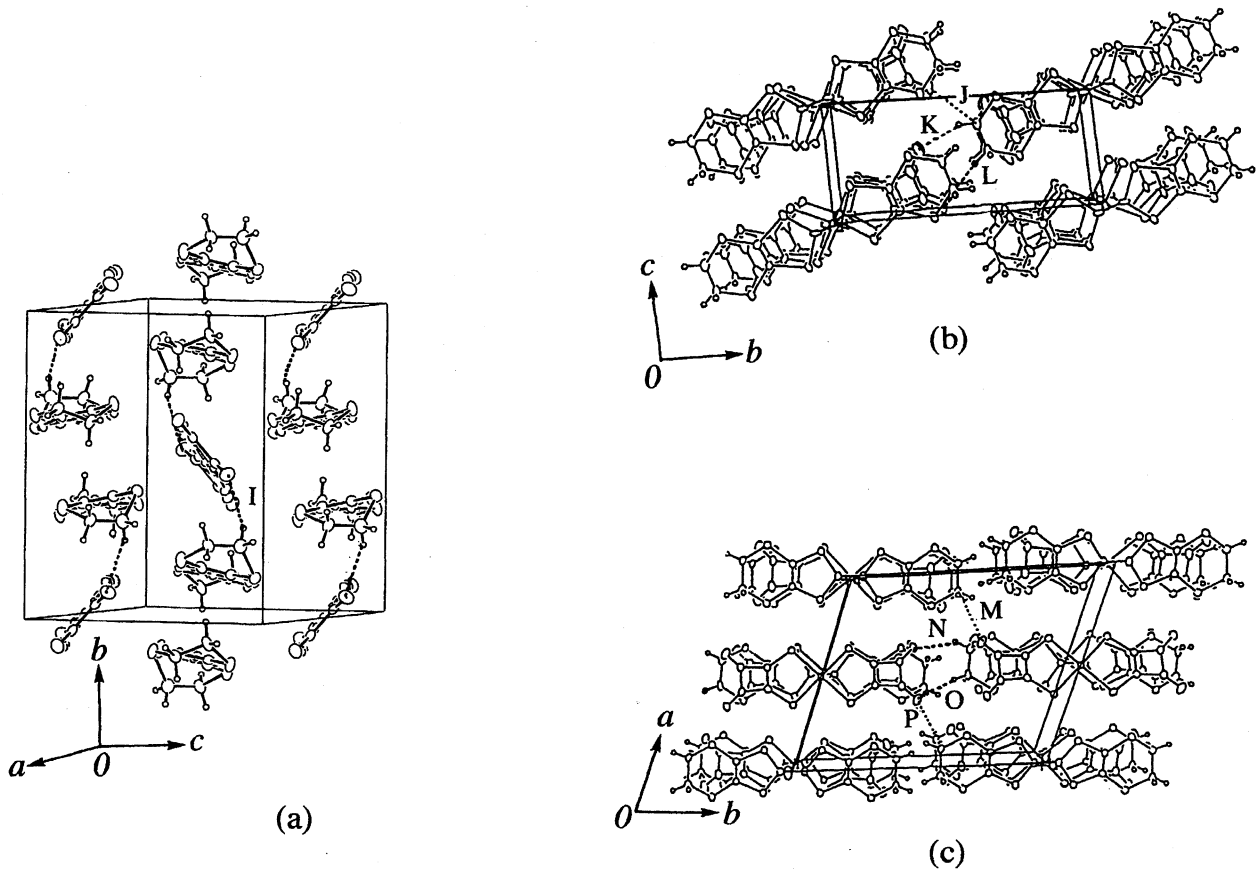

Fig. 10. C–H···O hydrogen bonds network in crystals, [C···O bond length/Å (C–H···O bond angles/°)]. (a) $(BETS)_2[Pd(dts)_2]\cdot 2(1,1,2,2\text{-TCE})$ (**2**), **I** [3.28(142.8)]. (b) $(BETS)[Au(dts)_2]$ (**4**), **J** [3.18(105.9)], **K** [3.29(152.1)], **L** [3.51(161.1)]. (c) $(ET)[Au(dts)_2]$ (**7**), **M** [3.47(132.0)], **N** [3.47(170.2)], **O** [3.19(144.3)], **P** [3.06(111.6)].

ductive salts, the resistivity ($\rho_{rt} = 2.5\ \Omega$ cm) and activation energy ($E_a = 100$ meV) of salt **4** are considerably smaller than those expected from its crystal structure of mixed stacks.

Charge on Donors. From the result of an XPS measurement, the Pd $3d_{5/2}$ core levels of salts **1**, **2**, **3**, and **5** are 338.0±0.4 eV, which are almost the same as that of $(TBA)_2[Pd^{II}(dts)_2]$ (338.1 eV). In the case of salt **6**, the Pt $4f_{7/2}$ core level is 73.7 eV, which is almost the same as that of $K_2[Pt^{II}(dts)_2]$ (73.9 eV). This means that the oxidation number of the palladium of salts **1**, **2**, **3**, and **5**, and the platinum of salts **6** are divalent. On the contrary, the Au $4f_{7/2}$ core levels of salts **4** and **7** are 86.2 and 86.4 eV, respectively, which are, to no small extent, deviated from that of $(TEA)[Au^{III}(dts)_2]$ (87.9 eV). Assuming that the oxidation number of gold of salts **4** and **7** is monovalent, the assessed charges on the donor are too large. This is not consistent with the discussion of bond lengths of donor molecules in the following. Therefore, it will be proper to consider that the oxidation number of the gold of salts **4** and **7** is trivalent. In fact, XPS is not so simple for ionic and conductive compounds. The ionicity and conductivity influence the Madelung energy and the relaxation time of electrons, and it often shifts the core level. The higher Au $4f_{7/2}$ core levels of $(TEA)[Au^{III}(dts)_2]$ would be due to these reasons.

However, it is evident that there is only one set of peaks, and no trace of two or more set of peaks about salts **1**, **2**, **3**, **4**, **5**, **6**, and **7**. This suggests that the oxidation numbers of the metal of these salts are not mixed valence states, but single states.

From cyclic voltammetry and chronocoulometry, an irreversible redox wave of $(Bu_4N)_2[Pd(dts)_2]$ is observed at +0.74 V (vs. SCE). As for $(Bu_4N)_2[Pt(dts)_2]$ and $(Bu_4N)_2[Au(dts)_2]$, the reversible redox waves are observed at +0.56 and −0.17 V, respectively, which correspond to the one-electron oxidation process ($[M^{II}(dts)_2]^{2-} \rightarrow [M^{II}(dts)_2]^- + e$ (M = Pd, Pt)) and the one-electron reduction process ($[Au^{III}(dts)_2]^- + e \rightarrow [Au^{III}(dts)_2]^{2-}$). However, it is impossible to isolate the oxidized or reduced products of bis(dithiosquarato)metalates by an electrochemical method. These one-electron redox processes suggest that the redox reactions occur mainly on the dts ligand moiety, and not the central metal, because the oxidation numbers of Pd^{III}, Pt^{III}, and Au^{II} are not stable.

Optical absorption measurements show the complete ionic character of salts **1**, **2**, **5**, and **6**, because there is no characteristic "A" band of the mixed-valence states.[28] However, as for salts **3**, **4**, and **7**, a new weak band appears around 8450, 8600, and 9550 cm^{-1}, respectively, which would be due to the mixed-valence states.

The charge assessed for donors is determined based on the valence of anions and the donor-anion stoichiometry. The intramolecular bond lengths of a donor are sensitively

Table 5. Electrical Resistivities at Room Temperature and Activation Energies

	1	2	3	4	5	6	7
	(BETS)$_2$[Pd(dts)$_2$]	(BETS)$_2$[Pd(dts)$_2$]·2(1,1,2,2-TCE)	(BETS)$_x$[Pd(dts)$_2$] ($x \approx 5$)	(BETS)[Au(dts)$_2$]	(ET)$_2$[Pd(dts)$_2$]	(ET)$_2$[Pt(dts)$_2$]	(ET)[Au(dts)$_2$]
ρ_{rt} (Ω cm)	2×10^3	5×10^3	0.025	2.5	1×10^3	5×10^3	1×10^4
Measured direction of resistivity	*a*-axis	*b*-axis	*b*-axis	*c*-axis	—	—	*c*-axis
E_a (meV)	185	220	Metallic	100	—	—	250
	Single cryst.	Single cryst.	Single cryst.	Single cryst.	Pellet	Pellet	Single cryst.

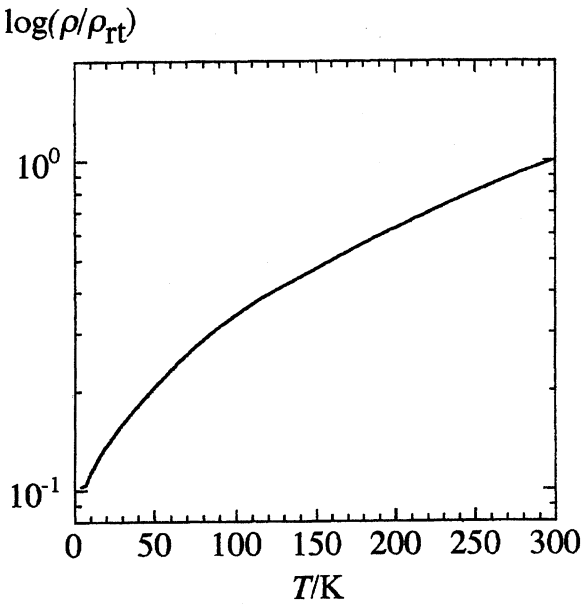

Fig. 11. Temperature dependence of the electrical resistivity of **3** salt.

effected by the charge on itself.[29,30] In ET salts, defining the average of four bond lengths between sulfur–carbon atoms of a five-membered-ring as *a*, and the average of three bond lengths between the carbon–carbon double bond as *b*, the ratio *b*/*a* is important for discussing the charge distribution on donors. The ratio *b*/*a* of salts **5** and **6** is 1.27 and 1.26 respectively, and the charges on the donor are estimated to be +1.[31,32] Concerning the charge on the ET molecule of salt **6**, C. Bellitto et al. concluded that +1 is assessed for the charge on ET from its stoichiometry, crystal structure and magnetism.[24]

On the other hand, the corresponding value of the BETS donor has not yet been studied. However, by adoption these methods on BETS salts, the corresponding *b*/*a* value of salts **1** and **2** are 1.39 and 1.39. From the result of XPS and cyclic voltammetry measurements of salts **1** and **2**, the charges on the donor of these salts are estimated to be +1.

An optical absorption measurement reveals the possibility of mixed valence states of salts **3**, **4**, and **7**. The charge on the donor of salt **3** is estimated to be +2/5, and its conducting behavior is metallic down to 4 K. From a discussion concerning the bond lengths of the donor, the ratio *b*/*a* of salts **4** and **7** are 1.28 and 1.45, respectively. These values are somewhat larger than those of salts **5** and **6**, and salts **1** and **2**, whose charges on the donor are estimated to be +1. However, considering the results mentioned above and their standard deviation of the bond lengths, the charges on the donor of salts **4** and **7** are estimated to be almost +1, but not completely ionic.

A series of cation of radical salts containing bis(dithiosquarato)metalate anions are not metallic conductors, except for salt **3**, because: i) they take kinds of mixed-stacked molecular arrangements and ii) the +1 oxidation states of the donors make them insulators. The probable reason for the mixed stacked structures of these salts is due to the strong ion-

icity of the donors and anions. The mixed-stacked molecular arrangements stabilize the lattice energy of ionic compounds by contributing the Madelung energy. In addition, the comparative similar sizes of the donors and anions make it easy to take mixed-stacked molecular arrangements.

However, the room temperature resistivity of salt **4** is rather lower than expected as a mixed-stacked cation radical salt. However, along the *c*-axis direction, the structure of salt **4** can be considered to form segregated columns; also, the low resistivity (2.5 Ω cm) was actually measured along the *c*-axis direction. Although an accurate resistivity measurement perpendicular to the *c*-axis direction was difficult to perform because of the size of the crystals, it may be about 10^3-times larger than that along the *c*-axis direction. The mixed-stacked charge-transfer salt (ET)[Ni(dmit)$_2$] shows a comparatively low electrical resistivity, and also has a large side-by-side transverse interaction of ET molecules.[11] In addition to the possibility of a mixed valence state, the low resistivity of salt **4** can also be explained by assuming that salt **4** has a large side-by-side transverse interaction of BETS along the *c*-axis direction. Actually, it is consistent with the comparatively large value of the overlap integral (60×10^{-3}) between side-by-side BETS molecules calculated based on the extended Hückel method. On the contrary, the high resistivity of salt **5** is explained by a small side-by-side transverse interaction of ET of salt **5**.

Conclusion

A series of cation radical salts of BETS and ET containing bis(dithiosquarato)metalate as an anion were synthesized. Most of their electrical resistivities except for salt **3**, showed semiconductive behaviors; though salt **3** exhibited a metallic behavior down to 4 K. It seems that the similar sizes of the donor and anion make it easy to take the mixed stacks in these cation radical salts, resulting in showing high resistivity. However, the salt **4** has stronger contacts between neighboring molecules along the side-by-side transverse direction than the molecular stacking direction, and shows low resistivity in spite of its molecular arrangement of mixed stacks. In addition, there are many C–H···O hydrogen bonds in these cation radical salts, which control the conformations of the ethylene groups of donor molecules.

The author thanks Dr. K. Ono (High power X-ray laboratory, the University of Tokyo), Mr. S. Terada, Professor T. Yokoyama, and Professor T. Ohta (School of Science, the University of Tokyo) for the measurement and the discussion of X-ray photoemission spectroscopy, and F. Sakai (Institute for solid state physics, and University of Tokyo) for the measurement of electron probe microanalysis.

References

1) See: J. M. Williams, J. R. Ferraro, R. J. Thorn, K. D. Carison, U. Geiser, H. H. Wang, A. M. Kini, and M-H. Whangbo, "Organic Superconductors," Prentice Hall, New Jersey (1992).

2) A. Kobayashi, R. Kato, T. Naito, and H. Kobayashi, *Synth. Met.*, **55-57**, 2078 (1993).

3) A. Kobayashi, T. Udagawa, H. Tomita, T. Naito, and H. Kobayashi, *Chem. Lett.*, **1993**, 2179.

4) R. Kato, H. Kobayashi, and A. Kobayashi, *Synth. Met.*, **41-43**, 2093 (1991).

5) H. Kobayashi, H. Tomita, T. Naito, A. Kobayashi, F. Sakai, T. Watanabe, and P. Cassoux, *J. Am. Chem. Soc.*, **118**, 368 (1996).

6) H. Tanaka, A. Kobayashi, T. Saito, K. Kawano, T. Naito, and H. Kobayashi, *Adv. Mater.*, **8**, 812 (1996).

7) P. Cassoux, L. Valade, H. Kobayashi, A. Kobayashi, R. A. Clark, and A. E. Underhill, *Coord. Chem. Rev.*, **110**, 115 (1991).

8) L. Brrossad, M. Ribault, L. Valade, and P. Cassoux, *Phys. Rev. B.*, **42**, 3935 (1990).

9) H. Tajima, M. Inokuchi, A. Kobayashi, T. Ohta, R. Kato, H. Kobayashi, and H. Kuroda, *Chem. Lett.*, **1992**, 1909.

10) A. Kobayashi, A. Sato, K. Kawano, T. Naito, R. Kato, H. Kobayashi, and T. Watanabe, *J. Mater. Chem.*, **5**, 1671 (1995).

11) A. Kobayashi, R. Kato, and H. Kobayashi, *Synth. Met.*, **19**, 635 (1987).

12) D. Coucouvanis, F. J. Hollander, R. West, and D. Eggerding, *J. Am. Chem. Soc.*, **115**, 4101 (1993).

13) D. Coucouvanis, D. G. Holah, and F. J. Hollander, *Inorg. Chem.*, **14**, 2657 (1975).

14) F. Götzfried, W. Beck, A. Lerf, and A. Sebald, *Angew. Chem., Int. Ed. Engl.*, **18**, 463 (1979).

15) J.-J. Bonnet, P. Cassoux, P. Castan, J.-P. Laurent, and R. Soules, *Mol. Cryst. Liq. Cryst.*, **142**, 113 (1987).

16) R. Kato, H. Kobayashi, and A. Kobayashi, *Synth. Met.*, **41-43**, 2093 (1991).

17) G. Maahs and P. Heigenberg, *Angew. Chem., Int. Ed. Engl.*, **5**, 888 (1996).

18) D. Eggerding and R. West, *J. Org. Chem.*, **41**, 3904 (1976).

19) "teXsan: Crystal Structure Analysis Package," Molecular Structure Corporation, (1985 & 1992).

20) C. D. Wagner, W. M. Riggs, L. E. Davis, J. F. Moulder, and G. E. Mullenberg, "Handbook of X-Ray Photoelectron Spectroscopy," Perkin–Elmer Corporation, Minnesota (1979).

21) H. Kobayashi, A. Kobayashi, Y. Sasaki, G. Saito, and H. Inokuchi, *Chem. Lett.*, **1984**, 183.

22) R. Kato, H. Kobayashi, A. Kobayashi, and Y. Sasaki, *Chem. Lett.*, **1984**, 1693.

23) R. Allmann, T. Debärdemäker, K. Mann, R. Matusch, R. Schmiedel, and G. Seitz, *Chem. Ber.*, **109**, 2208 (1976).

24) C. Bellitto, M. Bonamico, V. Fares, and P. Serino, *Inorg. Chem.*, **35**, 4070 (1996).

25) G. Saito, K. Yoshida, M. Shibata, H. Yamochi, N. Kojima, M. Kusunoki, and K. Sakaguchi, *Synth. Met.*, **70**, 1205 (1995).

26) G. R. Desiraju, *Acc. Chem. Res.*, **24**, 290 (1991).

27) A. Pénicaud, K. Boubekeur, P. Batail, E. Canadell, P. A-Senzier, and D. Jérome; *J. Am. Chem. Soc.*, **115**, 4101 (1993).

28) J. B. Torrance, B. A. Scott, B. Walter, F. B. Kaufman, and P. E. Seiden, *Phys. Rev., B*, **B19**, 730 (1979).

29) H. Kobayashi, R. Kato, T. Mori, A. Kobayashi, Y. Sasaki, G. Saito, T. Enoki, and H. Inokuchi, *Mol. Cryst. Liq. Cryst.*, **107**, 33 (1984).

30) K. Morimoto and T. Inabe, *J. Mater. Chem.*, **5**, 1749 (1995).

31) P. Guionneau, C. J. Kepert, G. Bravic, D. Chasseau, M. R. Truter, M. Kurmoo, and P. Day, *Synth. Met.*, in press.

32) K. A. Abboud, M. B. Clevenger, G. F. de Oliveira, and D. R. Talham, *J. Chem. Soc., Chem. Commun.*, **1993**, 1560.